ADDIS ABABA UNIVERSITY

ADDIS ABABA INSTITUTE OF TECHNOLOGY

SCHOOL OF CIVIL AND ENVIRONMENTAL ENGINEERING

PREDICTION OF SHEAR CAPACITY OF REINFORCED CONCRETE BEAMS BASED ON FRACTURE MECHANICS

A Thesis in Structural Engineering

By Nahom Kelemu Berile

November, 2021

Addis Ababa

A Thesis

Submitted in Partial Fulfillment of the Requirements for the Degree of Master of Science

The undersigned have examined the thesis entitled '**Prediction of Shear Capacity of Reinforced Concrete Beam based on Fracture Mechanics**' presented by **Nahom Kelemu**, a candidate for the degree of **Master of Science** and hereby certify that it is worthy of acceptance.

Dr.-Ing. Bedilu Habte		
Advisor	Signature	Date
Dr.-Ing. Adil Zekaria		
Internal Examiner	Signature	Date
Dr. Abrham Gebre		
External Examiner	Signature	Date
Chair person	Signature	Date

UNDERTAKING

I certify that research work titled “Prediction of Shear Capacity of Reinforced Concrete Beam based on Fracture Mechanics” is my own work. The work has not been presented elsewhere for assessment. Where material has been used from other sources it has been properly acknowledged / referred.

Nahom Kelemu

ABSTRACT

The determination of shear capacity of structural members without shear reinforcement in light of fracture mechanics has been a growing research interest ever since fracture mechanics theory for quasi-brittle materials including concrete has been developed.

In relations to fracture mechanics, size effect in reinforced concrete members is a phenomenon that is observed in experiments carried out to determine the load carrying capacity of structural members. With-increasing sizes of members, shear capacity is known to decrease at larger scale. It is the key objective of this research to assess whether or not such effect has been incorporated in the strength based approaches followed in the revised Ethiopian Building code and the building code by the American Concrete Institute. Furthermore, the research is aimed to evaluate the prediction power in the fracture mechanics based theories and have a further look into the strength based theories of analysis which, according to this research's findings, fail to incorporate the size effect.

This research selects 5 shear critical beams and uses the two building codes to estimate their shear capacity. After which a finite element model is prepared using the software ATENA 2D incorporating fracture mechanics based modeling techniques for the purpose of estimating the shear capacity of the same 5 beams examined using the building codes. From this study it was concluded that the two building codes lack to take the size effect into account and give a prediction that does not match experimental findings, especially for larger beam cross-section.

This study is not enough on its own to evaluate the lackings behind the shear capacity prediction formulas given by the two codes. Due to the fact that this research only has one variable parameter in the study, it is highly suggested that further researches be conducted in order to accurately test the fracture mechanics based theories and reconsider the code based approaches.

TABLE OF CONTENTS

LIST OF TABLES

LIST OF FIGURES

NOTATIONS

Roman upper case letters

A_s	reinforcement area
C	compressive force
E	Young's modulus
E_c	Young's modulus of concrete
E_s	Young's modulus of reinforcement
F	load
F_c	compressive force
F_s	tensile force
F_R	resisting force
G_F	fracture energy
L	length
P	load

Roman lower case letters

b	width
d	effective height
f_{ck}	compressive cylinder strength of concrete
$f_{c,cube}$	compressive cube strength of concrete
f_{yd}	yield strength of reinforcement
f_{ctd}	tensile strength of concrete
f_{yk}	characteristic yield strength of reinforcement
k	stiffness

Greek letters

ΔF	load increment
ε	Strain rate
ε_c	concrete strain
ε_s	reinforcement strain
ε_u	ultimate concrete strain in tension

θ	angle between cracks
ρ	reinforcement ratio,
σ	stress
σ_c	concrete stress
σ_s	reinforcement stress
σ_{sp}	tensile strength
σ_x	tensile stress in x-direction
σ_y	tensile stress in y-direction
τ	shear stress
ϕ	bar diameter
ν	poisson's ratio
ω_s	mechanical reinforcement ratio
γ_c	partial safety factor for concrete
γ_s	partial safety factor for steel

CHAPTER 1 INTRODUCTION

1.1 Background

Prediction of shear capacity of concrete members, reinforced and unreinforced, has been of a major interest in the concrete research world. The interest comes from both the practicing structural engineer's point of view in the need to avoid brittle failures which are premature failures ahead of attaining the member's maximum flexural strength and from the academic researcher's point of view longing to find a comprehensive approach to predicting shear capacity of structural members.

The fact that the shear capacity of a member depends on several factors including effective depth, beam width, shear span, aggregate size, longitudinal reinforcement, concrete strength and generally the size of the member among other things make the task even more challenging.

Among the factors affecting the shear capacity of a given concrete member, size effects are of this research's main interest. An increase in the overall depth of a beam with near minimum or no web reinforcement results in decrease in the shear stress at failure for a given longitudinal reinforcement ratio, concrete grade and shear span [2]. This shows that it is very crucial to take the size effect into account while determining the shear force capacity of concrete structures. However, most building codes do not provide a means of incorporating size effect in shear capacity determination. Furthermore, the strength based (stress and/or strain limit) approaches in analyzing structures lacks provision of objective (independent of mesh size and coordinate), energy based (crack absorption and ductility) principles [1]. Hence the need for adoption of fracture mechanics in the determination of shear capacity of reinforced concrete members, especially those with near minimum or no web reinforcements.

Among other factors, the size effect is, for design engineers, the most compelling reason for adopting fracture mechanics. Fracture mechanics being a recent development to the field of concrete structures is a center of many researches in relation with brittle failures. This research tries to use fracture mechanics theories and modeling techniques to assess their prediction power in determining the shear capacity of beams while addressing the

gaps in the area including lack of objectivity and compatibility with laboratory test results in the strength based analysis procedures.

1.2 Statement of Problem

Due to the reduction in shear capacity of relatively large reinforced concrete members with near minimum or no web reinforcements when compared to their lower scale counterpart, a method of prediction of the shear capacity which incorporates the size effect is important. Even though some of the building codes under practice, including the revised Ethiopian Code and the Euro code take the size effect into consideration, whether or not they give an accurate estimation of the shear capacity of members is probed by many researchers in the field [1]. A refined applicable approach for determination of maximum shear force at failure for shear critical large beams is crucial.

On top of this, fracture mechanics, being a recent advancement to the concrete world, provides a radical approach in determining crack initiation, formation and propagation characteristics in concrete members. However, building codes still use strength based approaches which fail to explain failure types associated with cracks, especially for large members [1].

Furthermore, even though stress (or strain) based approaches may give a reasonable means of determining load carrying capacities for smaller members, it is of a huge scientific importance to use energy based criteria when looked from the a scientific point of view. This is because actual formation of cracks requires certain energy – fracture energy and needs to be quantified with such parameter.

Hence, we can generally say, the lack of proper fracture mechanics based approach to shear capacity determination of large beams in building codes is the main initiation for this research.

1.3 Objective

1.3.1 General Objective

The aim of this research is to assess the prediction power of a fracture mechanics based modeling approach for prediction of shear capacity of reinforced concrete beams without web reinforcement.

1.3.2 Specific Objective

The research tries to provide a means of understanding the energy based criterion for shear design of beams.

Furthermore, the research attempts to evaluate the means of shear capacity estimation currently in practice and provide a better approach through the use of fracture mechanics modeling techniques implemented in recently developed software.

It is in this research's best interest to find a comprehensive means of estimating the shear capacity of beams by using a much more scientific-energy based approach that has been tested and found to be agreeable with experimental data.

1.4 Research Question and Hypothesis

Does the adoption of fracture mechanics theories in the prediction of shear capacity of beams without shear reinforcement give an enhanced approach in determining shear capacity of relatively large reinforced concrete members?

Through the implementation of fracture mechanics based cohesive crack models and crack band theory, an accurate estimation of shear capacity for reinforced concrete beams without shear reinforcement can be obtained.

1.5 Scope

This research is limited to:

- Reinforced concrete beams without web reinforcement
- Shear critical beams in order to make shear failure the governing failure mode

- Implementing a modeling approach that gives an accurate means of estimating the shear capacity of beams belonging to the above categories
- Fracture mechanics based cohesive crack models in an attempt to predict the shear capacity of the beams under consideration
- This research does not try to dig deep into already established strength based methods on their estimation of shear capacity of members

1.6 Methods and Procedures

The first step in conducting this research was collection of laboratory test results of shear critical beams without shear reinforcement. Laboratory tests conducted at an international level were gathered and officially published documents were used as an input for the research.

It is important to note that this research does not conduct any laboratory tests of its own in order to test the liability of the model outputs it formulates from a higher objective standard. The collected international laboratory tests on shear critical beams will serve as a basis for evaluation of the proposed modeling approach.

Having collected the laboratory test results of the beams, this research makes use of the ATENA software to model each beam aiming to find a modeling approach that incorporates the necessary theories of fracture mechanics to an end of estimating the shear capacity of the members under consideration.

Finally, the outputs of the proposed modeling approach were evaluated in light of the actual results from the laboratory tests conducted by other researchers and estimations of two building codes are compared and discussed.

1.7 Outline

This thesis is organized into five different chapters with the contents summarized as follows:

Chapter one, the introductory chapter, briefly describes the basics of fracture mechanics based approach to failures induced by shear. Furthermore, objectives of the thesis and the methodologies are briefly discussed under this chapter.

Chapter two, is an extensive literature study on the uncertainty of shear failure prediction and the adoption of fracture mechanics to quasi-brittle materials including concrete. Under this chapter, different fracture mechanics based modeling techniques proposed by several researchers including Bazant[1], Walraven [3], Jin-Keun Kim [4], Hillerborg [9], Roylance [6], Carpinteri [12] and Cervenka [5] are discussed. These theoretical and experimental works give practical insight into the challenges and means of approach to the adoption of fracture mechanics theories for concrete structures.

In chapter three, analytical computation of shear capacity determination of the sample beams selected for the purpose of this research is discussed largely. A total of 5 sample beams were selected with their depth as the varying parameter. The choice of the varying parameter was selected based on suitable criteria for the depiction of the significance of fracture mechanics based approach to the problem. The computation was carried out in three different approaches which include hand computations, excel program and Fortran program. The computations are based on two building code provisions. The Ethiopian Standards based on Euro Norms was one of the codes selected for this procedure and a building code with a different philosophy was included for the purpose of showing the different perspectives currently recommended for prediction of shear capacity of beams. Hence, the provision by the American Concrete Institute was selected to be the alternative approach in this chapter.

The fourth chapter presents the finite element model and its analysis results. The model was prepared using ATENA 2D software which incorporates fracture mechanics based modeling techniques. The results of this analysis are then compared with the code based computation results and the discussion of the results is presented at the end of this chapter.

Finally, the research summarizes its findings in the conclusion and recommendation chapter. The conclusions made in this chapter are all within the scope of the research and limited to the conclusive findings of this research. Recommendations are given for future studies in related areas through giving suggestions on the difficulties encountered while conducting the research.

CHAPTER 2 LITERATURE REVIEW

2.1 Shear in Reinforced Concrete Beams

Shear in reinforced concrete beams (RC Beams) is a means of internal stress for load resistance. Generally, a beam resists loads primarily by means of internal moments and shears. The stresses in an uncracked elastic beam reveal that shear stresses exist in those parts of a beam where the moment changes from section to section. The shearing stresses on an infinitesimal element with-in a given beam are equal on both the horizontal and vertical planes. The horizontal components are important in the design of construction joints, web-to-flange joints and regions adjacent to holes [2]. The shear stress distribution on a beam along a given section is shown below.

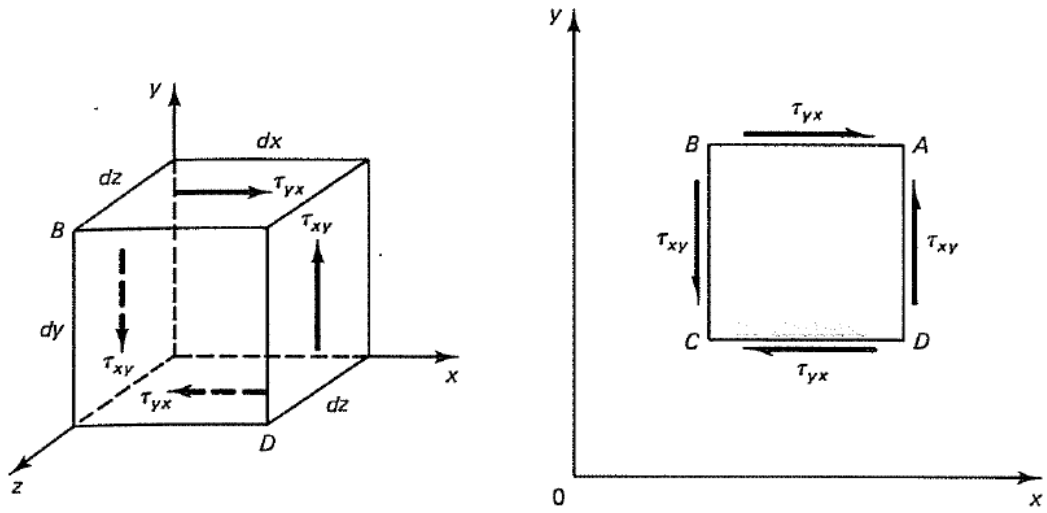

Figure 2-1: Shear stress distribution in a 3D and 2D element

Shear failures which are brittle relative to flexural failures are a major design constraint considered in design procedures. The manner in which shear failures occur varies widely with the dimension, geometry, loading, and properties of members.

2.2 Shear resistance in RC Beams without web reinforcement

The mechanism of shear resistance in reinforced concrete beams with and without web reinforcement has been discussed in great detail by R. Park and T. Paulay [17]. The shear strength of RC beams without web reinforcement are affected by the tensile strength of

concrete, the longitudinal reinforcement ratio, shear span-to-depth ratio, aggregate type, size of the beam, axial forces, and the aggregate size. [2]. Off of these factors, the dependency of the shear capacity of a beam on its size is this research's main interest. An increase in the overall depth of a beam with near minimum or no web reinforcement results in a decrease in its shear capacity at a given reinforcement ratio, shear span to depth ratio and concrete grade [2].

In the combined action of shear and flexure, a biaxial state of stress is induced in reinforced concrete members. With the tensile strength of concrete being exceeded, cracks form. In the conditions of high shear force, significant principal tensile stress at an angle of 45 degrees is created which are referred to as diagonal tension. The diagonal tension then results inclined cracks, the so called diagonal tension cracks. After the onset of such cracks, the tensile stress perpendicular to the crack surface drops to zero. The mechanism of shear transfer after the formation of such cracks differs in beams with and without web reinforcement.

In the absence of shear reinforcement, the total external shear force is resisted by the combined action of compression in the shear zone, dowel force transmitted across the crack, and vertical components of inclined shearing stresses transmitted across the inclined cracks by means of aggregate interlocks. [3]

In such beams several tests indicate that the contribution of the dowel action does not exceed 25% of the overall resistance [17]. The effect of dowel action is more significant when stirrups are used because flexural reinforcement can more effectively bear against a stirrup that is tightly bent around it.

A number of coarse aggregate particles projecting across a shear crack will enable small shear forces to be transmitted. The width of the crack, the roughness of the crack surface and the concrete strength contribute to this means of shear force transfer. The resistance from aggregate interlock is one of the major ones for the determination of shear resistance of a specimen. According to a series of beam tests conducted by a team under Park and Paulay [17], 50 to 70% of the shear resistance was from aggregate interlock mechanism.

The advancement of inclined cracks towards the compression zone reduces the "fixed end" of the hanging part of the cross-section from the compression zone. Once the dowel

action has been exhausted and the aggregate interlock has already been taken up by the external shear force, further crack propagation is inevitable. Such failure condition is referred to as diagonal tension failure [17].

Shear can also be sustained by inclined compression in a beam. Such resistance is called arch action and requires a substantial horizontal reaction at the support which then imposes heavy demands on anchorages. In real beams, the transition from beam action to arch action is gradual and can be determined based on the observation of the tensile stress on the reinforcement and variation of internal lever arm in test beams. One needs to be careful not to add the resistance contribution from the two actions because the deformations associated with the two mechanisms are incompatible. [3]

Arch action in beams is only limited to the case where loads are applied to the compression zone of the beam. The loading situation of a girder beam that supports secondary beams near its bottom edge belongs to the category of such cases. Beams whose resistance to shear comes from beam actions is the focus of this research.

2.3 Fracture Mechanics

2.3.1 Background

In 1983, the National Bureau of Standards of the United States of America and Battelle Memorial Institute estimated the cost for failure due to fracture to be $119billion per year. It is very hard to imagine the associated human life and injuries caused. [5] The term “fracture mechanics” refers to a vital specialization within solid mechanics in which the presence of a crack is assumed, and to finding quantitative relations between the crack length, the material’s inherent resistance to crack growth, and the stress at which the crack propagates at high speed to cause structural failure.

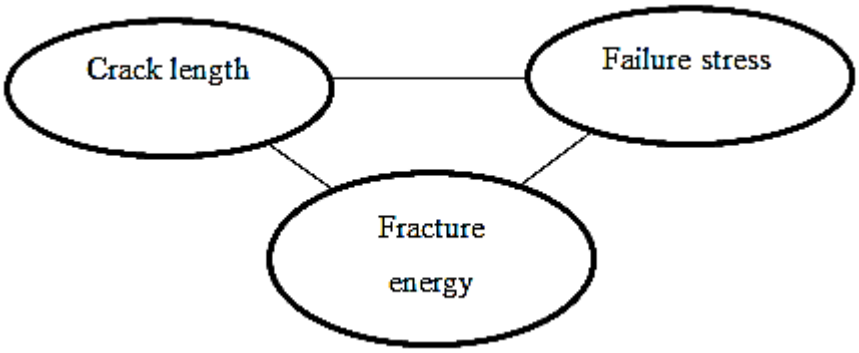

Figure 2-2: Main components of fracture mechanics

The pioneer work in the development of modern day fracture mechanics goes back to the beginning of the 20th century when Inglis [1] published a pioneer work on stress analysis for an elliptical hole in an infinite linear elastic plate loaded at its outer boundaries, in which a crack like discontinuity was modeled and stress singularity was observed at the crack tip.

For ideally brittle materials subjected to constant remotely applied stress, Griffith [1] presented the first explanation of the mechanism of brittle fracture using a new energy-based failure criterion. His theory was then extended to account for limited plasticity near the crack tip in majority of the engineering materials by Irwin and Orowan [2].

The adoption of fracture mechanics to the concrete world was then realized through the development of fracture mechanics based theory for quasi-brittle materials. Amongst the main reasons for the adoption of such theory is the size effect in concrete structural elements. The shear strength of beams without web reinforcement appears to decrease as the effective depth increases [17]. Dowel and aggregate interlock actions in particular can be considerably reduced especially if reinforcement bar sizes and aggregate sizes are not proportionally scaled.

This phenomenon is best explained using fracture mechanics, as put by Bazant and Kim [3] on the basis of energy release on cracking. The amount of energy released increases with an increase in size. Even though the theoretical basis for determination of the size effect and generally shear capacity of beams based on fracture mechanics already exists, there are several mismatches with experimental data on the subject matter. For that reason, other scholars in the field of concrete structures believe the size effect is best explained by the crack-width explanation instead of fracture mechanics. The works of

MacGregor show that in beams with at least the minimum required web reinforcement, the web reinforcement holds the crack faces together so that the shear transfer across the cracks by aggregate interlock is not lost. According to MacGregor, this is the reason behind the lack of significant reduction in shear strength in beams with minimum web reinforcement [2].

In the engineering practice it is the tensile strength that is used as the cracking criterion. However, the objectivity of such criterion has been under scrutiny several times due to the disagreement between analysis results and actual tests. Hence, it is necessary to study the energy based criterion.

2.3.2 Why Fracture Mechanics

From the physical point of view, crack initiation may depend on stress condition but actual formation of cracks requires certain energy – fracture energy. To disregard such relevant parameter would mean to ignore the science behind the mechanics.

The widely used approach to finite element analysis of concrete cracking is the concept of smeared cracking which in fact does not use the concept of fracture mechanics. However, it was observed that the approach lacks objectivity because of its incorrect convergence properties associated with the analyst's choice of mesh size; a problem known as spurious mesh sensitivity. When adopting the smeared crack modeling approach, the energy dissipated due to cracking decreases with the refinement of mesh sizes and converges to zero for very fine meshes. The only way to avoid such non-objective behaviour is by specifying the energy dissipated by cracking per unit length of the crack or the crack band. Hence, the fracture mechanic approach to crack initiation, formation and propagation in concrete elements provides objectivity than any other analysis approaches.

According to Bazant [1] the size effect is, for design engineers, the most compelling reason for adopting fracture mechanics. For obvious reasons most laboratory tests are conducted on small size concrete elements and it was common practice to scale the results observed to higher sizes. The size effect represents the deviation in such predictions and scaling techniques. Classical failure theories including the elastic analysis with allowable stress limit and plastic limit analysis put failure limits of stresses or strains independent of structure sizes and initial conditions (notched or not).

Furthermore, the ductility nature of structural elements also tends to show variations with structural sizes. With the classical approach this variation in the load carrying capacity of structural elements is not well predicted and hence the need for the adoption of fracture mechanics. It is due to the fact that in a larger structure more strain energy is available to derive the propagation of the failure zone.

2.3.3 Cracks and Energy Basis

Cracks are inevitable in concrete structures. In addition to their occurrences, most failures in concrete structures are associated with growth of cracking zones and formation of large fractures right before maximum loading is reached. Hence the need for a crack-propagation based approach to estimate the concrete capacities under different loading conditions.

In the presence of a crack the stress value cannot be used as a criterion of failure since the stress at the tip of a sharp crack in an elastic continuum is infinite no matter how small the applied load is.

Hence the need for energy based criterion. As primarily formulated by the late physicist Griffith [1], crack will propagate in a given solid specimen as long as the energy available to extend the crack by a unit surface area equals or exceeds the energy required to do so. This was the introduction of the concept of energy release rate.

However, most engineering analysis and design procedures are not based on fracture. Such theories developed for structural analysis use strength approaches which put limitations on the stresses (or strains) in concrete members. The first strength based approach was the development of elastic no-tension analysis during 1900-1930s, which was a major breakthrough in the world of concrete structures. Next to that was the plastic limit analysis, another strength based approach, which flourished in the 1940s. It is now believed that the introduction of fracture mechanics to the analysis and design of concrete structures might be considered the third breakthrough in the field.

The energy based approach of fracture mechanics makes it the most plausible for physicists and other scientists. [1]

2.3.4 Theoretical Basis for Fracture Mechanics

Most of the theories developed at the early stages of fracture mechanics and for several years after were for linear theories and could not be adopted for non-linear or quasi-brittle materials like concrete.

Grifith [1] was the pioneer in experimentally demonstrating the nominal strength of glass fibers increase when their diameter is decreased. The proposed idea was that these behaviors in isotropic solids came from the presence of discontinuities or flaws which statistically reduce when the member size is reduced. With this came the emergence of statistical size effect theories. From Mariotte, Tippett, Peirece, Fisher, von Mises and Weibull [1] the principles of statistical size effect were developed. It was in Weibull's conclusion that the tail distribution of low strength values of an extremely small probability cannot be represented by any of previously known distribution and introduced new statistical distribution that now bears his name.

Linear Elastic Fracture Mechanics is a valid theory only for macroscopically homogenous and linear materials. Due to the following two major properties encountered during fracture tests, the application of linear elastic fracture mechanics falls short [1]

- Slow crack growth, which reveals itself prior to unstable crack propagation
- Microcracking at crack tip, which itself is an energy absorption mechanism

It is important to introduce the concept of notch sensitivity for the discussion of dimensional analysis to follow. Notch sensitivity is the condition in which a notched specimen of a brittle material collapses mainly due to the stress concentration effect of the notch. In the notch sensitive case, the failure of the material is dependent upon the rupture stress due to the notch rather than the ultimate tensile strength. It has been observed that such conditions tend to disappear with a decrease in size [3].

Keeping in mind that the two potential causes of collapse are imminent in the specimen which are due to fracture and ultimate load, it can be asserted that, for brittle materials including plain or under-reinforced concrete, notch sensitivity is not an intrinsic material property, but it depends on the sizes of the structure where the crack is localized. The two potential collapses can be described as the collapse at ultimate strength, induced by

the highest normal stress in the body and the crack propagation collapse induced by the stress intensity factor. Hence, the discussions will focus on the two parameters, ultimate stress and stress intensity factor [3].

Let q_o be the load at collapse; in the simplest case of elastic-perfectly plastic material this ultimate load is a function of the geometric quantities and the stress intensity factor shown below:

$$q_o = q_o(\sigma_y, b, K_{IC}, F_p; \frac{a}{b}, \frac{t}{b}, \frac{l}{b}) \quad \textbf{(1-1)}$$

Where a is the crack length and F is the force of the plastic flow of the reinforcement.

The notch sensitivity is governed by a dimensionless quantity called the brittleness number, $S = \frac{K_{IC}}{\sigma b^{1/2}}$ and the relative crack length a/b. Hence, adding to the point that one of the potential failures which is related to fracture characteristics depend upon the size of the specimen [12].

Various nonlinear fracture mechanics theories were then brought forth by remarkable scientists from around the world. Amongst the developed theories elasto-plastic fracture mechanics with equivalent elastic crack models and cohesive crack models were the widely accepted ones.

Concrete shows its brittle nature in the structural size effect which implies that most results of concrete fracture experiments cannot be uniquely described by the commonly used strength of material approach. Even though linear elastic fracture mechanics captures the essence of size effect, it overestimates the load-bearing capacity of structures of usual dimension. The transition between the strength of material concept which is mainly stress based and the linear elastic fracture mechanics is nonlinear fracture mechanics [12]. Linear elastic fracture mechanics fails to describe the fracture properties of concrete unless it falls in the range of large sized structures like large gravity dams, but nonlinear fracture mechanics covers all reinforced concrete structures which are much smaller than dams and relatively within the building structural member sizes.

Crack propagation in concrete involves prior microcracking which is more or less concentrated in the highly stressed region ahead of the apparent crack tip. It is the heterogeneity of concrete that is responsible for the nonlinear fashion in a relatively large region adjacent to the apparent fracture front. The part of the nonlinear zone in which the material undergoes progressive microcracking is the fracture zone. [5]

Fracture energy is one of the most important parameters in the nonlinear fracture mechanics approach to the fracture failure of materials. It is the energy consumed by new surface formation. Experimental results have shown that the fracture energy depends on the maximum aggregate size and specimen dimension. In addition to the fracture energy value, the tensile softening diagram is also crucial in fracture analysis. The most direct way to determine the tensile softening diagram is through uniaxial tensile test which is very difficult to carry out. Hence, it is usual practice to use finite element analysis allowing the determination of a bilinear softening diagram from experimentally obtained load-displacement curves by means of a data fit [12].

The Blunt crack band theory being at the fore front of an energy based approach is discussed in detail by Bazant [10]. The hypothesis behind this theory is that in a heterogeneous material such as concrete fracture can be modeled as a band of parallel, densely distributed micro cracks having a blunt front.

For analytical purposes it is very important to approximate a given heterogeneous material by an equivalent homogeneous continuum. The stress and strain in his continuum shall be distinguished from that of the actual one. It is assumed that the Homogenized continuum stresses and strains are the averages of the microstresses and microstrains over a certain representative volume. Note that, even in the commonly practices approaches averaged material properties and the geometry of the microstructure with the differences in the elastic constants between the aggregate and the cement paste is not taken into account. Hence, this analogy can be used to justify the basic hypothesis of the Blunt crack band theory as follows. If in fact it is the averaged material property that is dealt with-in analysis procedures, it is then safe to assume that detailed distribution of stresses or strains over distances less than several times say the aggregate size is meaningless. Therefore, in case of fracture, if an equivalent homogenous continuum is assumed, it makes no sense to consider concentrations of stress (or of microcrack density) within volumes less that several aggregate sizes.

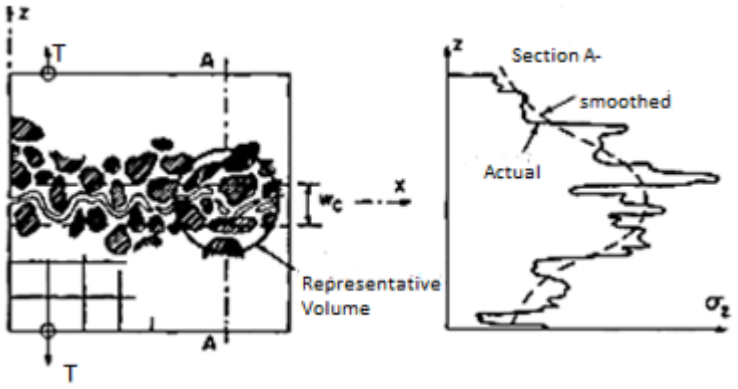

Figure 2-3: Approximation to a homogeneous continuum

Another assumption taken here is the approximation of cracks by straight lines. The actual crack path in concrete is obviously not smooth because of the aggregate pieces which result in random sways of the path. Such random sways are roughly equal to the aggregate sizes because such sways are actually due to the presence of the aggregates themselves. And as mentioned above, the actual stresses within such dimensions are insignificant and hence ignored in the macroscopic continuum model.

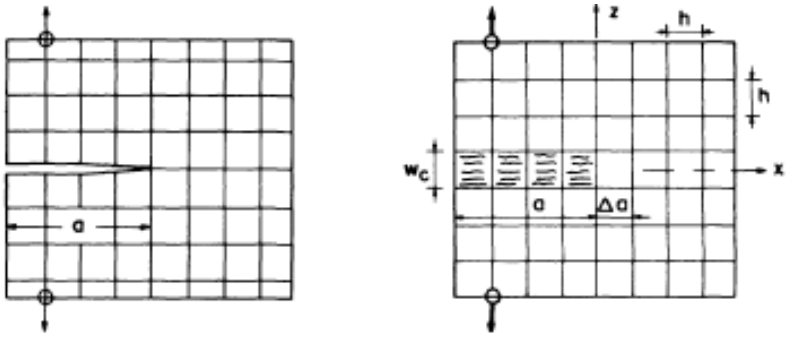

Figure 2-4: Crack Propagation Simulation Method

According to Bazant, for an elastic material in which the stress drops suddenly to zero at the fracture front, it is found that a sharp inter element crack and a smeared crack band in square mesh give essentially the same results for the energy release rate and agree closely with the exact elasticity solution. [10]

Hence, it can be concluded that because the line crack and the crack band models are essentially equivalent, a choice between these two only depends on computational preference.

Consider the case of using line cracks and a specific scenario where a crack crosses a single node which then results in the necessity of addition two new nodes in computation. Such continually occurring condition will demand higher computational capacity and hence is un-favored. Furthermore, when one is not able to determine the crack propagation direction, trial calculations are required for various possible nodes through which the crack should propagate is required making the job even more difficult.

The smeared crack approach by Rashid, as presented in Bazant's book [1], has a better solution to these difficulties by reducing the material stiffness in the direction normal to the cracks in the band. This also enables the modeling of crack propagation in an arbitrary direction or in a curved path simply by modeling the crack as zig-zag crack band whose overall path through the mesh approximates the actual crack path.

In this approach it is reasonable to assume the concrete outside the fracture zone behaves as nearly elastic because as opposed to ductile fracture in metals, where there is a large plastic zone in which the metal is yielding but does not go strain-softening, the nonlinear zone is not much larger than the strain-softening zone.

2.3.4.1 Stress-strain relation for fracture process zone

Having set the Cartesian coordinates for the analysis of stress and strain and keeping the strains with-in a very small limitation for linearized relation with the stress we can write the stiffness matrix of the uncracked material using the relation $\sigma = D^{*}\varepsilon$

$$D = \begin{pmatrix} D_{11} & D_{12} & D_{13} \\ & D_{22} & D_{23} \\ symm. & & D_{33} \end{pmatrix} \qquad \textbf{(1-2)}$$

Now assume that the elastic material whose stiffness matrix is developed above has been intersected by continuously distributed parallel cracks normal to z. The stress-strain relation will have to be modified to $\sigma = D^{fr} * \varepsilon$ where the fractured stiffness matrix is given by the following relation [10]

$$D = \begin{pmatrix} D_{11} - D^2_{13}D^{-1}_{33} & D_{12} - D_{13}D_{23}D^{-1}_{11} & 0 \\ & D_{22} - D_{23}D^{-1}_{33} & 0 \\ symm. & & 0 \end{pmatrix} \quad \textbf{(1-3)}$$

The development of the above stiffness matrix to an end of determining the stress-strain relation for fracture process zone is derived from the condition that the strain of the material between the crack is unrelated to the strain elsewhere except the fact that it is smaller. Furthermore, the stress normal to the cracks must be zero and it is assumed that the material between the cracks behaves as an uncracked elastic material. Even though these assumptions are somewhat unrealistic they are necessary for the analysis approach proposed.

The other option is, instead of continuously modifying the stiffness matrices, the elastic uncracked state can be represented using the compliance matrix as follows: $\sigma = C^* \varepsilon$

$$C = \begin{pmatrix} C_{11} & C_{12} & C_{13} \\ & C_{22} & C_{23} \\ symm. & & C_{33} \end{pmatrix} \quad \textbf{(1-4)}$$

After occurance of cracks along the z-axis, its effect is only manifested on the overall strain in that specific axis and not on the lateral strains. Hence, the modification on the compliance matrix becomes

$$C = \begin{pmatrix} C_{11} & C_{12} & C_{13} \\ & C_{22} & C_{23} \\ symm. & & C_{33}\mu^{-1} \end{pmatrix} \quad \textbf{(1-5)}$$

Bazant [10] refers to the coefficient as the cracking parameter. For a fully cracked material, the compliance matrix approaches the fractured stiffness matrix developed earlier. i.e.

$$D^{fr} = \lim_{\mu \to 0} C^{-1}(\mu) \quad \textbf{(1-6)}$$

With this, it is possible to study the transition from a crack-free state to a fully cracked state. At the crack free state the coefficient mentioned above has a value of 1.0 and at a fully cracked state 0. With the decrease in the cracking parameter, the stiffness matrix C implies that the stress in the strain in the member increases even while stress shows a gradual decrease. The gradual decrease of stress at increasing strain in concrete is what is referred to as strain softening.

How to govern the decrease in the value of the cracking parameter is a follow up question that deserves further clarification. Through a comparison of the stress-strain relation using the compliance matrix and a straight line softening assumption, the following relation has been published by Bazant [10]

$$\mu^{-1} = \frac{-C_{33}{}^{t}}{C_{33}} \frac{\varepsilon_z}{\varepsilon_o - \varepsilon_z} \tag{1-7}$$

Considering an isotropic concrete, we can write the compliance matrix as follows:

$$C(\mu) = \frac{1}{E} \begin{pmatrix} 1 & -\nu & -\nu \\ & 1 & -\nu \\ symm. & & \mu^{-1} \end{pmatrix} \tag{1-8}$$

Having determined the compliance matrix, the stiffness matrix can then be obtained by computing the limit of its inverse as the cracking parameter approaches zero

$$D^{fr} = \frac{E}{1-\nu^2} \begin{pmatrix} 1 & \nu & 0 \\ & 1 & 0 \\ symm. & & 0 \end{pmatrix} \tag{1-9}$$

It is assumed in the above formulation that the stress-strain relation in the vicinity of the fracture front is path-independent. Even though inelastic behavior in general is path-dependent this assumption has been proven to give rather sufficiently accurate result when compared with test data. However, more complicated approaches have been forwarded by other researches which take into account the path dependence.

2.3.4.2 Fracture energy

The energy consumed by crack formation per unit area of the crack plane is known as fracture energy. The fracture energy can be determined using the width of crack band (fracture process zone) and the work of tensile stress per unit volume.

From theoretical perspective, it may appear to be possible to determine the crack band width but in cases of large fracture process zone with non-homogeneously stressed specimen, it is quite complicated to do so. But that doesn't mean one can set the values of the work of tensile stress and the fracture energy as constants because that would imply that the crack band width is also constant.

2.3.5 Size Effect

Scaling, a quintessential problem of every physical theory is the change of response when the dimensions are scaled up or down while the geometry and all other characteristic are preserved. The effect of scaling on the strength of ropes was studied by Leonardo da Vinci. Even though the study of size effect in solid mechanics had started centuries ago, the scientific interest had fluctuated and has been keen only in the very recent history [7].

For linear elastic material and proportional loading, stress and strain relations remain within the proportional range and the failure remains within this range. Hence, material properties beyond the linearity range make no significance for the determination of failure characteristics. On the other hand, for elastic-perfectly plastic cases, the stress-strain relationships are not proportional in the neighborhood of the failure. The critical condition hence depends on the failure mode. The failures modes could either be governed by plastic flow which is a constant stress and strain level tending to infinity or by fracture which corresponds to vanishing stress and strain level tending to infinity.

For materials with aggregates, there is a range of stress relaxation beyond a certain strain level, which is referred to as strain softening. Even though several theories have been developed to describe these stress reductions with the observed strain values, most do not address the crack formation phenomenon which is one of the main sources of such behavior. Most of these theories describe progressive damage in concrete structures on an average manner but it is important to note that cracks are localized and anisotropic in nature.

Through mere observations in concrete tensile testing, it is possible to assert that the damage zone becomes highly localized with a decrease in loading capacity. It is also important to know that while the material in the fracture zone exhibits softening the rest of the material remains within the proportional limit; which perfectly explains why strains accumulate in the fracture zone while the remaining areas unload themselves. With this we can deduce that stress at softening stage depends on the fracture zone width w.

Having laid the foundation concept behind size effect, which is the dependence of the stress in the softening range on a fracture zone width w, it can readily be understood that the the descending branch of the stress strain curve is subject to size effect. It is also remarkable to see the fracture behavior of materials in the specific case of linear proportionality between the fracture zone width w and the structural size L.

As shown in figure 2-5 below, the area under the stress-strain curve represents energy dissipated per unit volume with a stress unit. On the other hand the area under a stress-fracture zone width curve represents energy dissipated per unit area with a unit of surface energy. More specifically, the area under this curve but limited to the stress softening range represents the fracture energy i.e. the energy necessary to create a unit surface. The transition from continuous to a discontinuous system requires the introduction of such quantities.

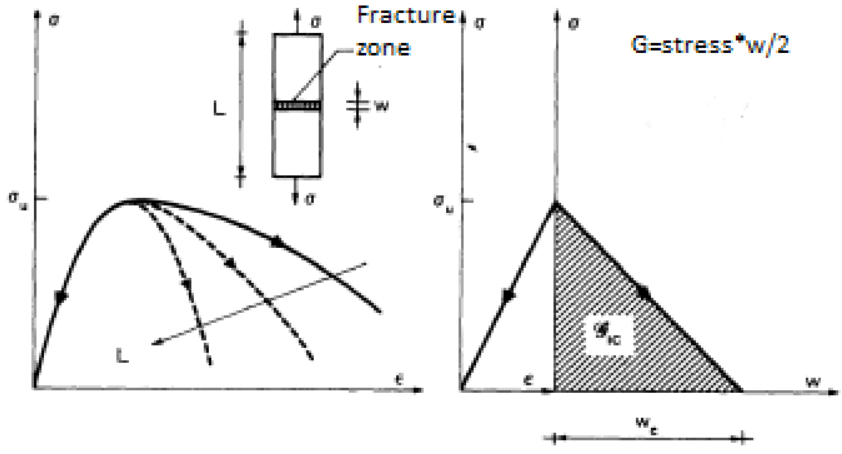

Figure 2-5: Graphical representation of fracture energy

When the sizes of the structural elements are small, the stress criterion tends to coincide with energy criterion. Therefore, just as the structural engineer should pay attention to

the importance of taking fracture criterion into account at significantly large sizes, the material scientist should also keep in mind that at lower ranges, the fracture criterions are just as good as, if not less, the stress criterions [4].

Until the mid-1980's, it was generally accepted that if a size effect is observed, it is of statistical origin as described by Weibull's theory [3]. Consequently, engineers and scientists gave no attention to mechanistic size effect. This is because the classically well-established theories of elasticity with strength limit showed no relation with size effect. The nominal strength of the structure does not depend on its size when geometrically similar structures are compared, was general belief until very recently.

Weibull's statistical theory is the traditionally accepted theory explaining the size effect in failure of concrete structure. According to this theory, size effect is due to the statistical distribution of the elements within the material under consideration. The reasoning for lowered strength in larger structures is explained by the statistical distribution of the aggregate (in the case of concrete) in the concrete specimen [6]. This is analogues to saying the survival probability of the structure is the joint probability of survival of all its elementary parts. But this is not easy to implement in analysis procedures for two-dimensional and three dimensional structures.

The simplest way of adopting fracture mechanics into the design practice of concrete structures is through the size effect. Modifying structural strength with the size of the structure is an approach used in most building codes.

When Kani [5] first observed the deviation in shear capacity of equivalent beams with varying depth (size) it was an eye opening to relook into the estimation of shear strength reinforced concrete members. The challenge in determining the shear strength of such members with significant size effect phenomenon was not just regarding the release of energy during fracture. Linear elastic fracture mechanics approaches would have been sufficient to do so. However, before failure, micro-cracking in the concrete causes deviations of the size effect from the geometrical size effect known from linear elastic fracture mechanics (LEFM), because for normal geometrical sizes the fracture process zone is relatively large with regard to the geometry of the structure and therefore the size effect can only be correctly calculated using nonlinear fracture mechanics (NLFM) [1].

In determining the punching shear resistance for slabs or column bases without shear reinforcement and shear capacity of beams and columns, the revised Ethiopian Building Code ES EN 1992:2015 and the European code EC-2 1992 has taken the size effect into consideration by introducing a coefficient, k.

$$k = 1 + \sqrt{\frac{200}{d}} \leq 2.0 \text{ d in mm} \qquad \textbf{(1-10)}$$

This equation shows the inverse relation of the shear capacity of the member under consideration with its effective depth.

2.3.5.1 Size Effect Sources

The concrete layer adjacent to the walls of the formwork has inevitably a smaller relative content of large aggregate pieces and a large relative content of cement and mortar than the interior member. In small structural elements, this portion occupies a large percentage of the overall structure while in large members, it is only a small part of the overall member size hence the difference between the two in load carrying capacity.

In addition to this, under normal stress parallel to the surface, the mismatch between the elastic properties of aggregate and mortar mix causes transverse stress in the interior. Another source of size effect due to near-surface conditions in concrete members is due to the Poisson effect (lateral expansion) causing the surface layer to nearly be in plane stress.

The other and most widely studied effect is due to randomness of material strength in concrete structures. Weibull has done a great deal of research in this matter.

Amongst these different explanations for the apparent experimental results affirming size effect, the focus of this research is on the explanation of size effect through the release of stored energy of the structure into the fracture front. This is in fact the most important source of size-effect [2].

2.4 Fracture Mechanics Modeling Techniques

Off of the mostly discussed modeling approaches which are based on fracture mechanics theories, we will try to review the Continuum models used together with fracture mechanics under this sub topic. Such a continuum model must be formulated in such a way that they are capable of describing fracture of the structure in a correct manner.

Even though the fore coming fracture mechanics modeling techniques gave good predications of failures only for brittle materials, nonlinear versions of the fracture mechanics theories were eventually developed. Amongst these are the equivalent elastic crack models, cohesive crack models and the crack band model.

2.4.1 Equivalent Elastic Crack Models

In equivalent elastic crack models, the nonlinear characteristics were represented by a decrease to the stiffness of the body or by an approximate increment in crack length while keeping everything else elastic. The name equivalent elastic crack is given to the extended crack induced in the material. This modeling approach is not within the scope of this research [13]

2.4.2 Cohesive Crack Model

In cohesive crack model, which is also referred to as fictitious crack model, the crack is assumed to extend and to open while still transferring stress from one face to the other. The distribution of these cohesive forces was to be calculated so that the stress singularity at the crack tip would disappear and the stresses would remain bounded everywhere.

The fictitious crack model proposed by Hillerborg for concrete needs not to be left without mentioning; most theories under this category require a preexisting crack to analyze failure conditions. Hillerborg included crack initiation rules for any situation while adopting most of the approaches in the cohesive crack model. The theory provides a continuous link between the classical strength based analysis of structures and the energy based classical fracture mechanics.

In determining shear strength of reinforced concrete beams, fictitious crack model has been widely used. The general principles are based on the concept that in pure tension, the material properties of a given element are described by means of the stress-strain

relation and the stress-displacement relation. The stress displacement relation is valid for a fracture zone which is around the fictitious crack. Such zone forms when the ultimate strain is reached. The strain outside the fracture zone remains below this limit, but the total deformation shall continue to increase depending on the displacement with-in the fracture zone. The remaining area outside this zone tends to unload as the displacement with-in increases. [8]

The fracture energy is, as briefly discussed earlier, the area below the stress-displacement curve. In other words, it is the energy absorbed when a unit area of a real crack is formed.

The fictitious crack in this model is generally assumed to transfer tensile stresses perpendicular to itself. Although the crack starts with a direction which is perpendicular to the main tensile stress direction when it first forms, further deformation of a structure may be such that sliding displacements and shear stresses also occur in the crack.

When shear and normal stresses act on the cracked regions, the principal tensile stress direction will no longer be perpendicular to the crack openings and hence will form a new crack at an angle to the previous one.

These secondary cracks are responsible for an unstable situation and a sudden collapse of the beam. This type of failure is referred to as diagonal tension failure [8].

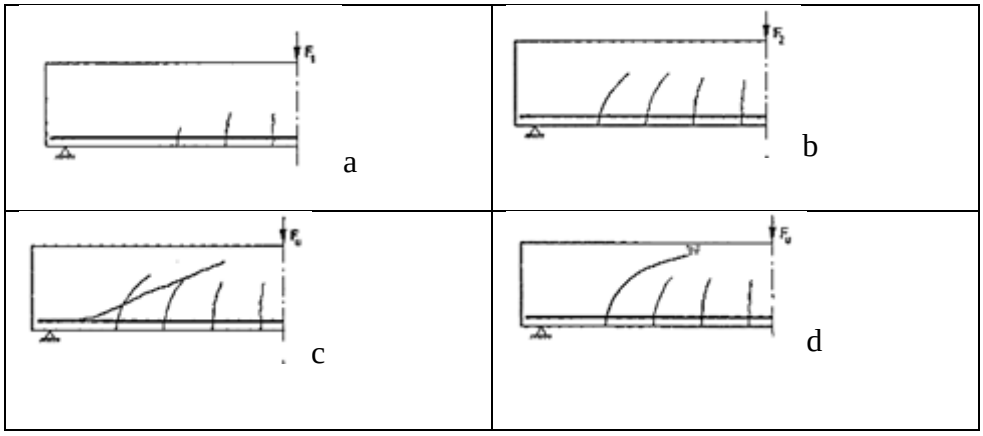

Figure 2-6: Crack propagation in diagonal tension failure (Where, a is flexural crack initiation; b is flexural crack propagation; c is diagonal crack development; d is diagonal shear failure.) [3]

On the other hand, if no secondary crack forms, the failure of the element will have to depend on the compression in the cracked region in which shear stresses are also acting. Hence, failure depends on combined effect of compression and shear leading to shear-compression failure.

In Gustafson's approach [9], only a single crack is assumed to exist in a given beam which is a shear crack and the propagation of this crack is assumed to lead to shear failure. The location of such crack formation is different in various beams. It is important to be able to determine the critical location of such crack formation and in this approach, the crack leading to the lowest failure load was taken to be the critical crack location.

The iteration of path of crack propagation is summarized in figure 2-7 below. Having set the location of the crack in such a manner, the paths of the crack propagation were iteratively determined with a bilinear or tri-linear shape.

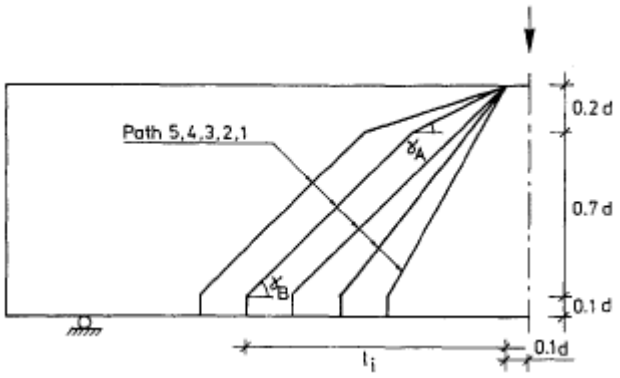

Figure 2-7: Iteration of path of crack propagation

The following assumptions were taken in the Gustafson's approach

- The stress-strain curves for concrete and steel are linear
- The descending stress-displacement curve for the stress transfer through the crack is linear
- The shear stress transfer through the crack has not been taken into account
- The bond-slip relation is elasto-plastic
- Dowel action is not taken into account
- The failure criterion in the compression zone is based on a modified Coulomb-Mohr criterion
- The shape of the beam is as shown in the figure below

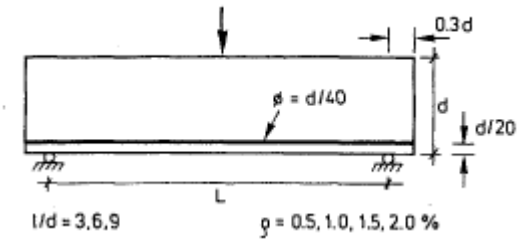

Figure 2-8: Beam Shape in Gustafson's approach

It is known that the crack starts at the bottom of the beam and propagates towards the top. In this approach it was observed that at first the load increases together with the crack length and the crack development is stable. However,, at a certain crack length an instability may occur. i.e the crack length may continue to increase with a reduction in loading. Moreover, as we continue in crack length increment, the load starts to increase once again, showing a stable crack propagation until failure occurs in the compression zone. For each beam, a different crack location has been considered and each time the final compression failure load has been taken as the maximum shear-compression failure resistance of the element.

This approach was then compared with actual test results and found to give reasonable output which fairly corresponds with test results. The main finding in this approach was that, the shear strength is actually proportional to the square root of the tensile strength as appose to the tensile strength itself. Most building codes tend to relate the shear strength with the tensile strength directly and such relation over estimates the shear strength of the member. The above result is under the assumption the fracture energy and the modulus of elasticity is not a function of the tensile strength of the concrete.

Another important take away from this is that the fracture energy is an important property for the determination of shear strength of beams. Its importance according to Gustafson may be just as that of the compressive strength of the concrete itself for the determination of shear capacity of members and other parameters too.

2.4.3 Crack Band Model

More theories emerged as more challenges to the application of fracture mechanics to concrete structure were faced. Bazant [1] proposed the crack band model as a solution to the size effect challenge faced in testing the fracture mechanics based theories which depict the characteristics of concrete structures at rather large scale. In the crack band

model cracks were simulated by a fracture band of fixed thickness and the strain was uniformly distributed across the band.

Strain softening behavior of concrete in the smeared-cracking framework was first introduced by Rashid. Afterwards, adapting to Hillerbord, Bazant and Oh [19] developed the crack band model in which the fracture process zone is modeled as a system of parallel cracks that are continuously distributed in the finite element. After the slight modification on the previously proposed micro plane model by Bazant and Prat [1], the following were set to be the basic hypothesis used in the crack band model.

Hypothesis I – The strains on any micro plane represent the resolved components of the macro strain tensor ε_{ij}.

Hypothesis II – Each micro plane resists not only normal strain but also shear strain. This shear strain is split into two mutually perpendicular in-plane components and as a consequence the shear stress vector is not parallel with the shear strain vector. This is the main modification in contrast to the originally proposed micro plane model where stress and strain vectors are parallel

Hypothesis III – The normal micro plane strain is splint into volumetric and deviatoric components

Hypothesis IV – The stress – strain relation for each micro plane is path independent as long as there is no unloading on this micro plane for that component. During each unloading and reloading, which is defined separately in each micro plane, the cures of the stress and strain differences from the state at the start of the unloading are also path independent. Thus, all the macroscopic path dependence is produced by various combinations of loading and unloading on all the micro planes.

Hypothesis V – The volumetric, deviatoric and shear responses on each micro plane are mutually independent. [7]

For the initiation of cracks in a body which originally is without cracks and stress concentrations, the concept of strength is acceptable for analysis and design of structural elements. However, when a sharp crack already exists in the element, the strength

approach fails to predict the behavior of the element. It incorrectly predicts the stress needed for the extension of a crack.

Therefore, it is in the conclusion of Bazant and Oh [19] that the elastic finite element analysis of cracking based on strength criterion, as currently used in computers is not objective in that it strongly depends on the analyst's choice of mesh. According to Bazant [1], such difficulty is only overruled by fracture mechanics.

It is still to be noted that even with the adoption of fracture mechanics theoretical basis, linear fracture mechanics also fails to appropriately predict the behavior of concrete elements. This deviation in concrete is due the heterogeneity of the material causing that it behaves nonlinearly within a relatively large zone adjacent to the fracture front which goes beyond the scope of linear fracture mechanics.

Because of computational convenience as well as resemblance to reality, the cracking of concrete is usually modeled in finite element software as a system of parallel cracks that are continuously distributed (smeared) over the finite elements. The hypothesis of blunt crack band model is in general the hypothesis that in a heterogeneous material can be modeled as a ban of parallel, densely distributed microcrakcs with a blunt front. [20]

The justification for the adoption of the blunt crack band approach is presented as follows:

The first justification comes from the notion of adopting representative volume. When a heterogeneous material is approximated by an equivalent homogenous continuum, it is important to differentiate between the continuum stresses and strains and the actual stresses and strains. The cross section of this volume should ideally be taken to be much larger than the size of the inhomogeneities and even for a crude modeling must be considered to be at least several times the maximum aggregate size in the case of concrete [1].

Consequently, the distribution of stress or strain over distances less than several aggregate sizes has no physical meaning. Only the stress resultants and accumulated strain over the cross sections of the characteristics volume do. Hence, to use finite elements less that several aggregate sizes makes no sense. Therefore, one should not attempt to subdivide the width of the crack band front into several finite elements.

The second justification point is from equivalence of results, based on experimental results presented in the paper published by Bazant [20] for an elastic material in which the stress drops suddenly to zero at the fracture front, it was found that a sharp inter-element crack band and a smeared crack bang give essentially the same results for the energy release rate and agree closely with the exact elasticity solution provided that the finite element is not larger than about 1/15 of the cross section dimension.

Finally reasoning for the adoption of the blunt crack band is the computational advantage. In the line crack approach when the crack extends through a certain node, the node must be split into two nodes, increasing the total number of nodes and changing the topological connectivity of the mesh. Unless all nodes, are renumbered the band structure of the structural stiffness matrix is destroyed. All of this complication is avoided through the adoption of the blunt crack band model.

The actual pattern of micro cracks is observed at the fracture front in most experiments and from these observations the larger micro cracks are not spread over a band of a large width but are concentrated essentially in a line However, the line along which the micro cracks are scattered is not straight (or smoothly curved) but is highly tortuous. This scatter in the locations of visible micro cracks relative to a straight line characterized by a micro crack band better than by a straight row of micro cracks.

The width of the fracture process zone is assumed to be constant in this approach. For normal concrete it is usually taken to be three times the aggregate size. The crack band width is set to constant in order to avoid spurious mesh sensitivity. The fracture energy is then related to the crack band with by the energy dissipation due to fracture per unit length of crack, which is also a constant in this approach.

The figure below represents a crack band model specimen under uniaxial tension, with fracture process zone width and crack length represented as h_c and a respectively.

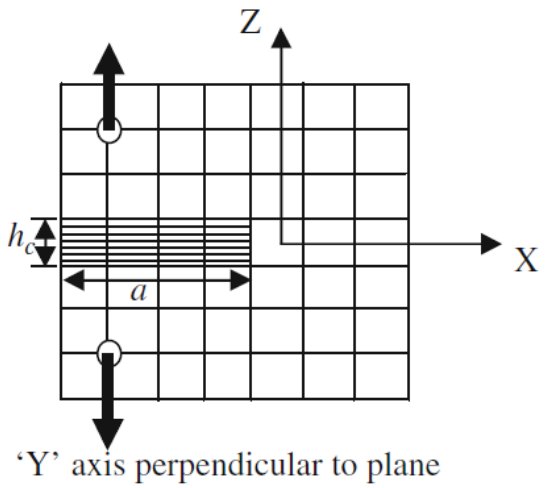

Figure 2-9: Cartesian coordinate representation of crack band model

In this approach, the crack is modeled by changing the isotropic elastic moduli matrix to an orthotropic one, thereby reducing the stiffness in the direction normal to the cracking panel.

A mathematical basis for the crack band model has been forwarded by Bazant and Oh [19] by considering a system of cateriesian coordinates. Assuming the concrete is idealized as a homogenous material, the triaxial stress-strain relationship can be expressed as:

$$\begin{Bmatrix} \varepsilon_x \\ \varepsilon_y \\ \varepsilon_z \end{Bmatrix} = \frac{1}{E}\begin{pmatrix} 1 & -\nu & -\nu \\ -\nu & 1 & -\nu \\ -\nu & -\nu & 1 \end{pmatrix}\begin{Bmatrix} \sigma_x \\ \sigma_y \\ \sigma_z \end{Bmatrix} + \begin{Bmatrix} 0 \\ 0 \\ \varepsilon_f \end{Bmatrix} \qquad \textbf{(2-11)}$$

Where the sigma's are the principal stresses and the epsilons is the principal strain except for the final strain component, ε_f is the fracture strain by the opening of the micro cracks. As the micro cracks develop in the material the effect of these micro cracks does not cause any change in the strains in the X and Y directions. The fracturing strain is determined by summing all the deformation of individual cracks.

Fracture starts when the stress at the crack tip reaches the tensile strength; at which point the fracture strain still remains zero. As the crack opens the fracture deformation starts to

gradually increase and the principal strain in the corresponding direction declines. This enables the development of the relationship between the principal strain and the fracturing strain as follows:

$$\varepsilon_f = f(\sigma_z) = \frac{1}{C_f}(f_t - \sigma_z)$$
$$C_t = \frac{f_t}{\varepsilon_o} \quad \textbf{(2-12)}$$

Where:

ε_f is the fracture strain by the opening of the micro cracks

ε_o is the strain at the end of strain softening

f_t is the tensile strength of concrete

C_t is the fracture coefficient associated with tensile strain

C_f is the fracture coefficient associated with the fracture strain

Here, ε_o is the strain at the end of strain softening at which the micro cracks coalesce into a continuous crack and the principal stress vanishes. It is at this point that the earlier stress-strain relationship is revised:

$$\begin{Bmatrix} \varepsilon_x \\ \varepsilon_y \\ \varepsilon_z \end{Bmatrix} = \frac{1}{E} \begin{pmatrix} 1 & -\nu & -\nu \\ -\nu & 1 & -\nu \\ -\nu & -\nu & \frac{E}{E_t} \end{pmatrix} \begin{Bmatrix} \sigma_x \\ \sigma_y \\ \sigma_z \end{Bmatrix} + \begin{Bmatrix} 0 \\ 0 \\ \varepsilon_o \end{Bmatrix} \quad \textbf{(2-13)}$$

As shown in the matrix representation, the post-peak tensile stress-strain relationship is described by the tangent modulus E_t which is defined as:

$$\frac{1}{E_t} = \frac{1}{E} - \frac{1}{C_f} \leq 0 \quad \textbf{(2-14)}$$

For finite element analysis, the stress-strain relation mentioned above must be inverted to get the stiffness matrix. This matrix is particularly simple for the case of plane stress analysis.

We can conclude that the basic requirement is to represent the heterogeneity in the actual specimen in our model. While doing so, the interaction among particles and damage sites in the microstructure must include interactions at a distance among various sites and interactions among various orientations.

It is the interaction among various sites that is well presented in the nonlocal approach. The nonlocal approach is a requisite for a realistic description of the size effect, as well as for the modeling of fracture propagation in the form of crack band.

In the nonlocal approach, stress at a point doesn't necessarily depend on strain at that same point but also on the strain field in a certain neighborhood. Within the modified approach, so called nonlocal continuum with local strains, the characteristic length is the key parameter. This is the length over which the stress is averaged due to the significance in the influence on the results. Even though previous researches had understand this characteristic length to be correlated with the fracture energy or other material properties, latest findings confirm that these parameter is not just related with material property but also the strain conditions in the failure zone, hence making it difficult to determine its value.

2.5 Fracture Mechanics Based Finite Element Modeling

The effect of cracks can be simulated by nonlinear finite element analysis. The scope of application for complex nonlinear analysis is aimed at development of new technical solutions of anchors, special loading types and investigation of failure cases and it is not meant for normal design. [13]

There are three non-linear material properties that need to be taken into account in the effort of implementing the fracture mechanics based approach; the crack band model based on fracture energy, fracture plastic model with non-associated plasticity and micro plane material model.

The crack band model based on fracture energy is of main interest for this specific research. Concrete without cracks is isotropic but one with cracks is considered to be orthotropic with the option of modeling the orthotropic axes as rotated or fixed cracks. The rotated crack option aligns the crack with the principal strain direction and the fixed cracks once aligns the crack in the principal strain direction at the onset of cracking and makes no change to it. It is in the fixed crack option where the model of shear becomes important whereas the rotated crack option a shear on the crack plane never appears and the shear model need not to be employed.

The above mentioned modeling techniques cannot be applied for post-peak range because post-peak softening is structure dependent and a simple strain-based model is not objective for such considerations.

The specific software chosen for this research - ATENA has incorporated the fracture mechanics approach based on the crack band model and fracture energy is implemented. [13]

It is also one of the very important characteristic of the software when selecting it for this research that the crack band approach employed for tensile and compressive softening avoids the finite element mesh sensitivity. The nonlinear finite element package ATENA is based on advanced constitutive models.

The prediction contest for strength of 4m deep concrete slab strip set forth by the University of Toronto in Canada was won by incorporating fracture mechanics based modeling techniques [14]. Their prediction was found to be the best among other 66 entries from all over the world. This accurate prediction was achieved with a numerical analysis based on nonlinear constitutive model of concrete using fracture mechanics.

In the published paper about their prediction [14] the authors have mentioned that the commercial software ATENA was used in the research. This was another factor when selecting a suitable software for the research. The core of the simulation software is a constitutive model of concrete, whose validation was continuously performed through numerous project and bench marks, including this specific contest under consideration.

Vladmir Cervenka in his conference paper on Fracture Mechanics of concrete and concrete structures presents their winning prediction for a large beam tested at Toronto

University [4]. The crack propagation was modeled by a smeared crack approach and a fracture mechanics based cohesive crack model. The fact that the prediction was the closest from all the contestants with its fracture mechanics oriented approach gives an additional support to the adoption of fracture mechanics in analysis of shear critical beams.

The fracture plastic constitutive mode is the numerical analysis incorporated in the finite element software developed by the authors. The major principles in the fracture plastic constitutive mode are

- Strain decomposition into damage components that include elastic, plastic, fracture and other damages
- Smeared crack model with crack band localization limited and fixed cracks
- Compressive stress reduction as a result of tensile cracks

The numerical analysis has incorporated incremental analysis with iteration in each step by the Newton-Raphson method. Specific to the model prepared for the contest, the reinforcements were modeled by truss elements embedded in the concrete elements and a perfect bond between the two was assumed.

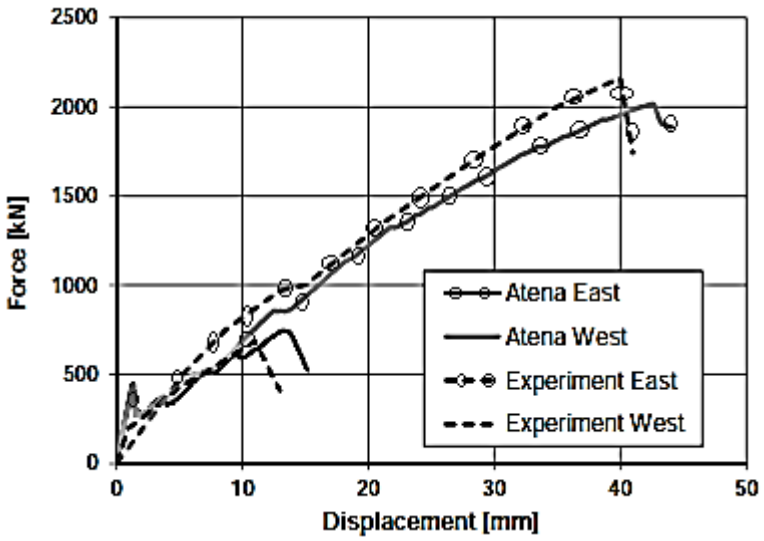

Figure 2-10: ATENA prediction and actual test comparison

Following the contest the authors performed an investigation of a model uncertainty paid special attention to parameters that take into account the aggregate interlock. The shear factor, a parameter that relates shear fracture mode II to the crack opening fracture mode

I is the main parameter that takes into account the effect aggregate interlock. When considering low shear factor in numerical analysis, it may significantly affect the analysis output up to changing the failure mode. Instead of a diagonal crack a system of strut and tie can be formed. Consequently the tensile failure due to a diagonal crack changes to compressive failure and hence leads to a higher resistance. Shear of the crack face for shear strength has a significant impact on determining the strength of the specimen.

In order to incorporate this effect in numerical models, the usage of rotated crack approach is recommended by the authors [14]. However, the rotated shear crack option is based on the assumption that there occurs no shear stress on cracks; which is why the fixed crack approach was favored by the contest winners.

A mesh sensitivity study was also conducted after the submission of the prediction. It was observed that for square mesh sizes varying from 50mm to 400mm for linear and quadratic elements the error was within a range of 12%. Even though it is true that larger meshes show less error, this underlines the fact that fracture mechanics based approaches have lower mesh sensitivity.

CHAPTER 3 ANALYTICAL CALCULATION

3.1 Reinforced Concrete Beam Samples

For this specific study a reinforced concrete beam that was used in 'Prediction contest for strength of four meter deep reinforced concrete slab strip' organized by M.P. Collins and E.C. Bentz from the university of Toronto [18] is taken as the first reference beam in order to study the fracture mechanics based way of predicting the shear strength of reinforced concrete beams.

Even though the beam used at the Toronto contest had shear reinforcements on one of its shear span; the scope of this research is limited to the portion that is without such reinforcements. In this chapter, we will use analytical means of determining the shear capacity of reinforced concrete members that is based on the revised Ethiopian Building code; Ethiopian Standard - Based on Euro norm, Design of Concrete Structures – Part 1.1 and the American Concrete Institute provision for shear capacity determination.

In order to understand the relation between size and fracture mechanics based means of determining the shear capacity of reinforced concrete beams, the depth of the beam used at the Toronto contest is gradually reduced in both analytical calculations and finite element models prepared. This gives the research ability to compare the predicted shear capacities of the corresponding beams in code based approach and the fracture mechanics based finite element models.

Furthermore, having shown the detail analytical computations for few of the sample beams, data from fortran V.97 program prepared for all of the beams incorporated in this study is included in the annex.

The table below shows the different beam samples with their corresponding depths that are to be used in this research. The beam width, concrete grade, support condition, span and tensile reinforcement are kept constant for each beam sample.

Table 3-1: Common parameters of the sample beams

Parameter	Value
Beam width	0.25m
Concrete grade (f_{cu})	37MPa
Reinforcement grade (f_{yk})	400MPa
Support condition	Simply supported
Span	24m
Tensile reinforcement	9ϕ30 in 3 layers
Loading	Concentrated Load at Mid Span

Table 3-2: Variable parameters of sample beams

Beam Label	Beam depth (m)	a/d (Shear span to beam depth ratio)
Beam – 1 (Toronto)	4	3
Beam - 2	3.5	3.43
Beam - 3	3	4
Beam - 4	2.5	4.8
Beam - 5	2	6

The choice of the parameter to vary has been broadly discussed in the literature review. The purpose in choosing to vary the beam depth alone while keeping all other parameters constant is to study the size effect and the importance of using fracture mechanics based modeling techniques in determining the shear capacity of large reinforced concrete beams.

As discussed in the first chapter of this document, the scope of this thesis is limited to beams that develop resistance to shear through beam action only. Furthermore, the beams under study are also shear critical beams as the major objective of this research is focused on beam shear capacities. With this two limiting factors, the maximum and minimum limit of the beam depth was decided based on the relations between shear span to depth ration and failure modes in concrete beams presented by MacGregor [2].

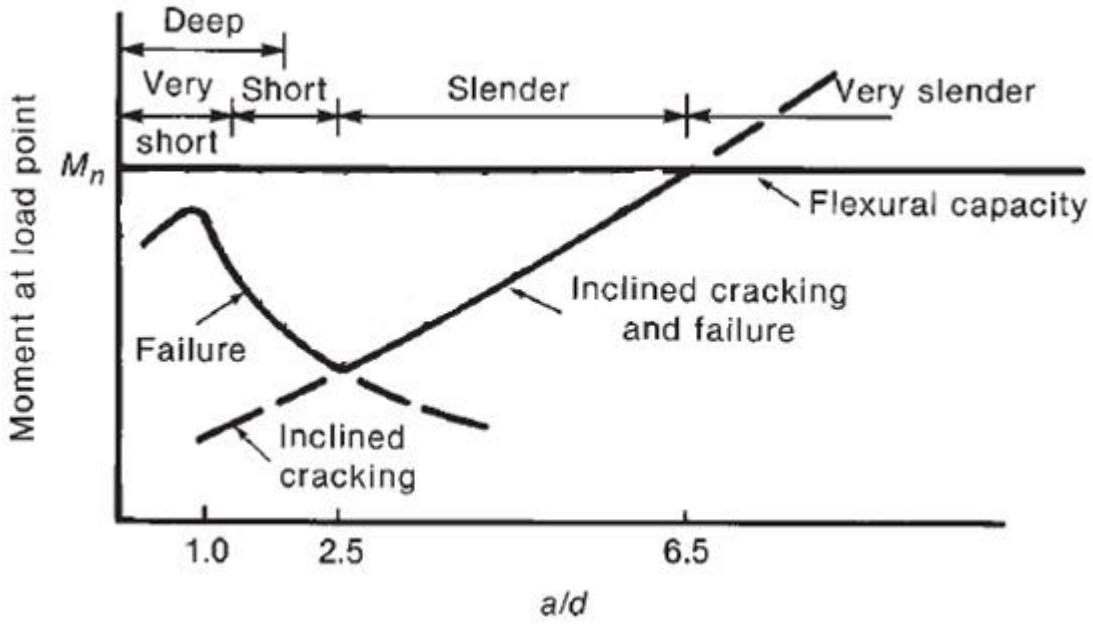

Figure 3-11: M_n as a function of a/d [2]

While the sample beams remain in the slender beam category according to the above filure, their failure mode is limited to incline cracking which is due to shear. It is within these limiting boundaries that the depth of the sample beams is set to vary between 4m and 2m.

In addition to the sample beams listed above, it was found necessary to also analyze and discuss sample beams as a verification of the software itself and the fracture mechanics based modeling approach implemented. Ten sample beams were modeled analyzed to this end. Below is the list of these beams together with their important specifications. The sample beams were taken from a publication by M. P. Collins [26] which presents 1547 beams tested in the United States between 1948 and the date of the publication.

Table 3-3: Verifying beam properties

Beam ID	Beam name on publication	Beam width B_w (mm)	Beam depth h (mm)	Effective depth d (mm)	Distance of load point from support center (mm)	Beam Span (mm)
V-Beam 1	Leonhard's	190	320	283	810	1960
V-Beam 2	Walraven's	200	750	720	2160	4320
V-Beam 3	Kani's	154	1219	1095	2737	5474
V-Beam 4	Toronto	250	4000	3895	12000	24000
V-Beam 5	Regan's	400	100	83	450	900
V-Beam 6	Batson's	102	152	127	610	1220
V-Beam 7	Taylor's	400	1000	930	2800	5600
V-Beam 8	Niwa's	600	2100	2000	6000	12000
V-Beam 9	Johnson's	305	610	539	1670	3340
V-Beam 10	Kawano's	600	2200	2000	6000	12000

Beam ID	reinforcement ratio ρ	reinforcement area A_s (mm^2)	maximum aggregate size d_a (mm)	Concrete cylinderical strength f_c' (MPa)	Reinforcement yield strength f_y (MPa)	Maximum observed shear force V_{ult} (kN)
V-Beam 1	0.0197	1059.27	-	28.5	400	96.28
V-Beam 2	0.0079	1137.60	16	23.2	440	226
V-Beam 3	0.0270	4553.01	19	26.4	375	237
V-Beam 4	0.0065	6329.38	-	37	400	685
V-Beam 5	0.0166	551.12	10	37.8	670	62.5
V-Beam 6	0.0310	401.57	19	34.7	276	19.2
V-Beam 7	0.0135	5022.00	38	28.7	420	358.4
V-Beam 8	0.0028	3360.00	25	27.1	999	402
V-Beam 9	0.0025	409.34	19	55.9	525	191.5
V-Beam 10	0.0120	14400.00	40	23.1	400	560

3.2 Fracture Mechanics Based Approach

It is to this date a unanimous fact that the shear failure of reinforce concrete beams is a very complex fracture phenomenon for which a purely mathematical approach is not possible [20]. However, mathematical approaches that take into account fracture mechanics parameters and specifically the size effect do not necessarily demand detailed modeling of fracture mechanism. Bazant and Yu have dealt with the formulation of such

approach in their two fold paper [20]. The implementation of the crack band theory discussed extensively in the literature review is presented in the fourth chapter.

In the development of the mathematical approach the size effect is measured in terms of nominal strength, generally defined as:

$$\sigma_N = P/bd \qquad \textbf{(3-15)}$$

Where P is the maximum ultimate load

The size effect is characterized by comparing the nominal strength for geometrically similar structures of different sizes d. In the classical allowable stress design and the limit state design, the nominal strength is independent of the structure size. The case has now come clear that design formulas must include the size effect.

The lack of adequate test data, especially at large element sizes has made it literally impossible for the development of empirical formula for determination of a mathematical relation that takes fracture mechanics into account.

Even though problems of quasibrittle fracture in normal range of interest are very difficult to solve, the asymptotic properties are simple and can be exploited. The plastic limit analysis gives an accurate estimation of behaviors of concrete elements of relatively smaller sizes. Whereas, linear elastic fracture mechanics – which is a theory in which the fracture process zone is a small point gives accurate estimation of concrete elements of larger sizes. Such theory is proved to give sufficient result for excessively large members (in ranges of 100m depth).

Based on these asymptotic relations, Bazant and Yu [20] have formulated the following relation for the determination of shear capacity of reinforced concrete members. This relation will be adopted here for the estimation of the shear capacity of the selected beam samples.

$$V_{Rd,c} = [0.2\rho^{3/8}(1+d/a)\sqrt{f_c'}(1+d/d_o)^{-1/2}]b_W d$$
$$d_o = 694\sqrt{d_a}\,(f_c')^{-2/3} \qquad \textbf{(3-16)}$$

Where:

d is the effective depth of the beam

ρ is the longitudinal reinforcement ration

$$\rho = \frac{A_{sl}}{b_W d} \leq 0.02$$

A_{sl} is the area of the tensile reinforcement

b_W is the smallest width of the cross-section in the tensile area [mm]

a is the shear span of the beam

f_c' is the cylindrical strength of the concrete

d_o is the length parameter of size effect parameter

d_a is the maximum aggregate size

Beam - 1

For the first sample beam, Beam – 1 (Toronto) the shear capacity is determined as per the simplified formula given by Bazant and his team [20] according to equation (3.16).

$f_c' = 40MPa$

$d = D - x$; where x is the distance to tensile reinforcement centroid measured from the bottom of the beam cross section.

Assuming there are 3 bars in each layer and there is a clear distance of 30mm between the layers of the reinforcement and also assuming a reinforcement cover of 30mm.

$$x = \frac{3*(30+\frac{30}{2})+3*(30+30+30+\frac{30}{2})+3*(30+30+30+30+30+\frac{30}{2})}{9}$$

$$x = \frac{135+315+495}{9}$$

$$x = 105mm$$

Therefore;

$$d = D - x$$

$$d = 4000mm - 105mm$$

$$d = 3895mm$$

$$a = 12,000mm$$

$$\rho_l = \frac{A_{sl}}{b_W d} \leq 0.02$$

$A_{sl} = 9*\frac{\pi*30^2}{4} = 6361.73mm^2$ is the area of the tensile reinforcement

$$\rho_l = \frac{A_{sl}}{b_W d} \leq 0.02$$

$$\rho_l = \frac{6361.73}{250*3895} = 6.328*10^{-3}$$

$$b_W = 250mm$$

$$\sigma_{cp} = 0$$

$$d_o = 694\sqrt{d_a}\left(f_c'\right)^{-2/3}$$

$$d_a = 20mm$$

$$d_o = 694\sqrt{20}\left(40\right)^{-2/3}$$

$$d_o = 265.36$$

$$V_{Rd,c} = [0.2\rho^{3/8}(1+d/a)\sqrt{f_c'}(1+d/d_o)^{-1/2}]b_W d$$

$$V_{Rd,c} = [0.2(6.328*10^{-3})^{3/8}(1+3895/12000)\sqrt{40}(1+3895/265.36)^{-1/2}]*250*3895$$

$$V_{Rd,c} = [0.2(0.15)(1+0.325)*\sqrt{40}*(1+14.678)^{-1/2}]*973,750$$

$$V_{Rd,c} = [0.2(0.15)(1.325)*\sqrt{40}*0.253]*973,750$$

$$V_{Rd,c} = 619348.5N$$

$$V_{Rd,c} = 619.4kN$$

The shear capacity of the first sample beam – Beam – 1 (Toronto) is 619.4kN.

The shear capacity determination of the rest of the sample beams is presented in the annex of this document. The summary the results for all the beams are shown below:

- $V_c = f(d_{eff}, b_w, \rho_l, a, d_a, f_{cd}, f_{ctd}, \ldots)$

Table 3-4 : Summary of predictions based on Bazant's Equation

Beam Label	Cross-section	$V_{Rd,c}$ according to Bazant's Equation
Beam - 1	250mmX4000mm	619.4kN
Beam - 2	250mmX3500mm	592.8kN
Beam - 3	250mmX3000mm	560.1kN
Beam - 4	250mmX2500mm	529.3kN
Beam - 5	250mmX2000mm	484.2kN

3.3 Code Based Approach

3.3.1 Shear Capacity of Reinforced Concrete Beams – ES EN 1992

3.3.1.1 Analytical Calculation

According to the Ethiopian Standard – Based on Euro Norm, the design value for the shear resistance of members not requiring design shear reinforcement is given by the relation:

$$V_{Rd,c} = [C_{Rd,c}k(100\rho_l f_{ck})^{1/3} + k_1\sigma_{cp}]b_W d \quad \textbf{(3-17)}$$

With a minimum of

$$V_{Rd,c} = [v_{\min} + k_1 \sigma_{cp}] b_W d$$

Where:

f_{ck} is in MPa

$$k = 1 + \sqrt{\frac{200}{d}} \leq 2.0 \text{ with d in mm}$$

$$\rho_l = \frac{A_{sl}}{b_W d} \leq 0.02$$

A_{sl} is the area of the tensile reinforcement

b_W is the smallest width of the cross-section in the tensile area [mm]

$$\sigma_{cp} = \frac{N_{Ed}}{A_c} < 0.2 f_{cd} \text{ [MPa]}$$

N_{Ed} is the axial force in the cross-section due to loading or prestressing [in N]

A_c is the area of concrete cross section [mm^2]

$V_{Rd,c}$ is in [N]

The code also specifies the recommended values for the remaining parameters in the equation to be as follows:

$$C_{Rd,c} = \frac{0.18}{\gamma_c}$$

$$k_1 = 0.15$$

$$v_{\min} = 0.035 k^{3/2} f_{ck}^{1/2}$$

Beam - 1

For the first sample beam, Beam – 1 (Toronto) the shear capacity is determined as follows as per the Ethiopian Standard – Based on Euro Norms.

$$V_{Rd,c} = [C_{Rd,c} k (100 \rho_l f_{ck})^{1/3} + k_1 \sigma_{cp}] b_W d$$

Where:

$$f_{ck} = 40MPa$$

$$k = 1 + \sqrt{\frac{200}{d}} \leq 2.0 \text{ with}$$

$d = D - x$; where x is the distance to tensile reinforcement centroid measured from the bottom of the beam cross section.

Assuming there are 3 bars in each layer and there is a clear distance of 30mm between the layers of the reinforcement and also assuming a reinforcement cover of 30mm.

$$x = \frac{3*(30+\frac{30}{2}) + 3*(30+30+30+\frac{30}{2}) + 3*(30+30+30+30+30+\frac{30}{2})}{9}$$

$$x = \frac{135+315+495}{9}$$

$$x = 105mm$$

Therefore;

$$d = D - x$$
$$d = 4000mm - 105mm$$
$$d = 3895mm$$

$$k = 1 + \sqrt{\frac{200}{3895}} \leq 2.0$$
$$k = 1.227$$

$$\rho_l = \frac{A_{sl}}{b_W d} \leq 0.02$$

$A_{sl} = 9 * \frac{\pi * 30^2}{4} = 6361.73 mm^2$ is the area of the tensile reinforcement

$$\rho_l = \frac{A_{sl}}{b_W d} \le 0.02$$

$$\rho_l = \frac{6361.73}{250 * 3895} = 6.533 * 10^{-3}$$

$$b_W = 250 mm$$

$$\sigma_{cp} = 0$$

$$C_{Rd,c} = \frac{0.18}{\gamma_c} = \frac{0.18}{1.5} = 0.12$$

$$k_1 = 0.15$$

$$v_{\min} = 0.035 k^{3/2} f_{ck}^{1/2}$$
$$v_{\min} = 0.035 (1.227)^{3/2} (40)^{1/2}$$
$$v_{\min} = 0.3$$
$$V_{\min} = 0.3 * 250 * 3895$$
$$V_{\min} = 292125 N$$
$$V_{\min} = 292.12 kN$$

$$V_{Rd,c} = [C_{Rd,c} k (100 \rho_l f_{ck})^{1/3} + k_1 \sigma_{cp}] b_W d$$
$$V_{Rd,c} = [0.12 * 1.227 (100 * 6.533 * 10^{-3} * 40)^{1/3} + 0] 250 * 3895$$
$$V_{Rd,c} = 0.432 * 973750$$
$$V_{Rd,c} = 420470 N$$
$$V_{Rd,c} = 420.47 kN$$

The analytical calculation for the rest of the beams is presented in the annex.

In a similar manner, the shear capacity of the remaining beams is calculated using a simple excel spread sheet and a Fortran V.97 program prepared for the purpose of this research.

Table 3-5: Beam - 1 Shear Capacity - ES EN

Beam shear capacity

BEAM - 1 (Toronto)

Beam cross section	
B (mm)	250
H (mm)	4000
x	105
Cover (mm)	30
d (mm)	3895
Beam Concrete Grade	
f_{cu} (Mpa)	50
f_{ck} (Mpa)	40
f_{cd} (Mpa)	22.67

$C_{Rd,c}$	0.12
k	1.2267
k_1	0.15
Beam Tensile Reinforcement	9 ϕ 30
A_s (mm^2)	6361.73
ρ	0.006533227
σ_{cp} (Mpa)	0
v_{min} (Mpa)	0.3008
$V_{Rd,c}$ (N)	420661.251
$V_{Rd,c}$ (kN)	425.367

The numerical program findings for the rest of the beams are presented in the annex.

Table 3-6: Summary of predictions based on ES EN

Beam Label	Cross-section	$V_{Rd,c}$ according to ES EN Prediction
Beam - 1	250mmX4000mm	420.7kN
Beam - 2	250mmX3500mm	393.2kN
Beam - 3	250mmX3000mm	359.3kN
Beam - 4	250mmX2500mm	323.2kN
Beam - 5	250mmX2000mm	284.2kN

3.3.2 Shear Capacity of Reinforced Concrete Beams – ACI 318 – 08

3.3.2.1 Analytical Calculation

According to ACI provisions, the shear strength is calculated based on an average shear stress on the full effective cross section $b_w d$. For members without shear reinforcement, shear is assumed to be carried by the concrete web in the ACI. Furthermore, the shear strength provided by the concrete is taken as the shear causing significant inclined cracking.

Furthermore, for areas in B-regions (Flexure governed regions or beam regions) the traditional shear design procedure is acceptable which ignores D-regions.

The shear capacity computation is presented in the 11th chapter of the code, chapter 11 – Shear and Torsion. ACI 318 – 08, 11.2.1.1 states that for members subject to shear and flexure only, the shear strength provided by the concrete is:-

$$V_c = 2\lambda\sqrt{f_c'}b_W d \qquad \textbf{(3-18)}$$

Where λ is, according to ACI 318 – 08, 8.6.1 a modification factor for all-light-weight and sand-light-weight concrete. For normal weight concrete λ = 1.0. Furthermore, the code also specifies that if the average splitting tensile strength of the lightweight concrete is specified λ is given by a formula in the specific clause of the code mentioned above.

Since the sample beams under study are all composed of normal weight concrete, the value of λ is set to be 1.0.

$V_c = 2\sqrt{f_c'}b_W d$

According to ACI 318 – 08, 5.1.2 f_c' shall be based on test of cylinders made and shall be based on 28-day tests. Hence, f_c' corresponds to the cylindrical strength of the concrete in Psi unit. As per the specification mentioned at the beginning of this project the, the corresponding value for f_c' is taken as 40MPa, which is the same as 5801.51psi.

In the more detailed approach for shear capacity determination of reinforced concrete beams without shear reinforcement, section 11.2.2.1 of ACI 318 – 08 recommends the following detailed calculation

$$V_c = (1.9\lambda\sqrt{f_c'} + 2500\rho_W \frac{V_u d}{M_u})b_W d \qquad \textbf{(3-19)}$$

But not greater than

$$V_c = 3.5\lambda\sqrt{f_c'}b_W d \qquad \textbf{(3-20)}$$

In the commentary under R11.2.2.1 it is stated that it is convenient to assume that the second term in parenthesis in the detailed equation is equal to $2500\rho_W \frac{V_u d}{M_u} = 0.1\sqrt{f_c'}$ allowing the analysis procedure to follow the simplified approach mentioned above.

Beam – 1 (Toronto)

$$V_c = 2\sqrt{f_c'}b_W d$$

$$V_c = \frac{2\sqrt{5801.51psi} * 9.843" * 153.347"}{1000 lb/kip}$$

$$V_c = 229.922kip$$

$$V_c = 1022.74kN$$

The shear capacity of the first sample beam – Beam – 1 (Toronto) is 1022.74kN.

The analytical calculation for the rest of the beams is presented in the annex.

In a similar manner, the shear capacity of the remaining beams is calculated using a simple excel spread sheet and a Fortran V.97 program prepared for the purpose of this research.

Table 3-7: Beam - 1 Shear Capacity - ACI

Beam shear capacity	
BEAM - 1 (Toronto)	
Beam cross section	
B (in)	9.843
H (in)	157.481
x (in)	4.134
Cover (in)	1.181102
d (in)	153.3465
Beam Concrete Grade	
f_{ck} (psi)	5801.52
$V_{Rd,c}$ (kip)	229.9334
$V_{Rd,c}$ (kN)	1022.79

The results of the numerical program for the rest of the beams are presented in the annex. Below is the summary of all the ACI based beam shear capacity predictions.

Table 3-8: Summary of predictions based on ACI's Equation

Beam Label	Cross-section	$V_{Rd,c}$ according to ACI Prediction
Beam - 1	250mmX4000mm	1022.7kN
Beam - 2	250mmX3500mm	891.5kN
Beam - 3	250mmX3000mm	760.2kN
Beam - 4	250mmX2500mm	628.9kN
Beam - 5	250mmX2000mm	497.6kN

The results of all of the above discussed predictions are summarized in the table below:

Table 3-9: Summary of predictions based on Bazant's Equation, ES EN and ACI codes

Beam Label	Cross-section	$V_{Rd,c}$ according to Bazant's eqn. prediction	$V_{Rd,c}$ according to ES EN Prediction	$V_{Rd,c}$ according to ACI Prediction
Beam - 1	250mmX4000mm	619.4kN	425.3kN	1022.7kN
Beam - 2	250mmX3500mm	592.8kN	393.2kN	891.5kN
Beam - 3	250mmX3000mm	560.1kN	359.3kN	760.2kN
Beam - 4	250mmX2500mm	529.3kN	323.2kN	628.9kN
Beam - 5	250mmX2000mm	484.2kN	284.2kN	497.6kN

Beam ID	$V_{Rd,c}$ according to Bazant's eqn. prediction (kN)	$V_{Rd,c}$ according to ES - EN prediction (kN)	$V_{Rd,c}$ according to ACI prediction (kN)
V-Beam 1	93.87	45.47	47.67
V-Beam 2	228.8	69.57	115.59
V-Beam 3	243.6	119.76	143.88
V-Beam 4	609.9	414.8	983.6
V-Beam 5	36.212	31.6	33.9
V-Beam 6	12.674	14.78	12.67
V-Beam 7	350.65	221.11	330.97
V-Beam 8	443.59	372.47	1037.4
V-Beam 9	100.3	87.82	204.12
V-Beam 10	506.1	573.65	957.84

CHAPTER 4 FRACTURE MECHANICS BASED FINITE ELEMENT ANALYSIS

4.1 Introduction

Finite element method is a numerical technique to determine approximate solutions for boundary value problems, for partial differential equations and also for integral equations. Finite Element Analysis (FEA) represents a numerical method, which provides solution to problems that would otherwise be difficult to obtain. The finite element analysis to the sample beams discussed in the preceding were performed using ATENA 2D, a nonlinear finite element analysis program that utilizes two-dimensional continuum elements. This software is a suite of powerful engineering simulation programs, based on finite element method, which can solve problems ranging from relatively simpler linear analyses to the most challenging non-linear simulations. The reason behind the choice of this specific software, as discussed in the first chapter, is to make use of fracture mechanics based failure theories that are buil-in the software program.

In this chapter, the nonlinear finite element analysis of the sample beams computed in Chapter 3 is discussed.

4.2 Modeling Basis

Ahead of directly going into the finite element model and analysis outputs, the fracture mechanics modeling approach used in this model is discussed in depth. The Crack Band Theory and Cohesive crack model approach to nonlinear fracture mechanics of concrete elements is adopted in the software used. The modeling assumptions and simplifications are discussed below:

4.2.1 Material Model

The material model in the software carefully chosen for this research includes the following aspects of concrete behavior

- Non-linear behavior in compression including hardening and softening

- Fracture of concrete in tension based on nonlinear fracture mechanics
- Biaxial strength failure criterion
- Reduction of compressive strength after cracking
- Reduction of the shear stiffness after cracking and
- Two crack models: fixed crack direction and rotated crack direction

The nonlinear behavior of concrete in the biaxial stress state is described by means of the so called effective stress and the equivalent uniaxial strain. In most cases, this effective stress is the principal stress. Below is shown the complete equivalent uniaxial stress-strain diagram for concrete material definition in the model:

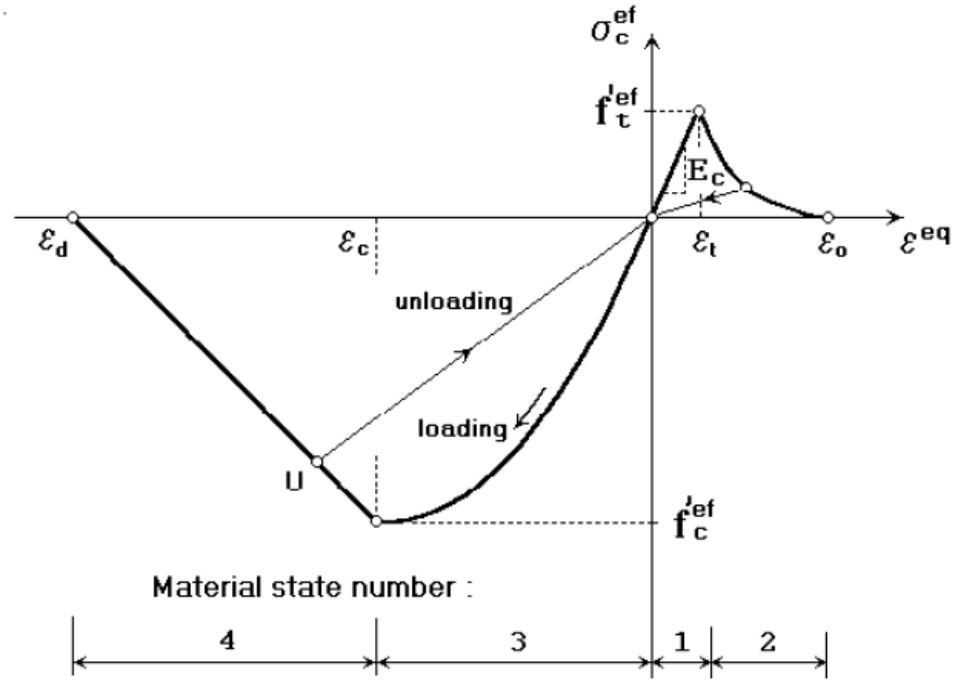

Figure 4-12: Stress-strain diagram for concrete material definition in ATENA Software [4]

The behavior of concrete in tension without cracks is assumed linear elastic. However, as for tension after cracking there are two types of formulations. Off of the two types, only one of them is used here.

The adopted cracking formulation type is a fictitious crack model based on a crack-opening law and fracture energy. This formulation is suitable for modeling of crack propagation in concrete and it is used in combination with the crack band modeling approach.

The localization limiter built-in in the software controls the localization of deformations in the failure state. It is a band of material which represents a discrete failure plane in the finite element analysis. In tension it is a crack and in compression it is a plane crushing. In the case of tensile cracks, the approach knows as the crack band theory which has been discussed in depth in the literature review is directly adopted. The purpose of the adoption of the failure band is to eliminate two deficiencies, which occur in connection with the application of the finite element model: element size effect and element orientation effect.

The process of crack formation is treated in three stages in the models discussed under this chapter. The uncracked stage is the one before the tensile strength is reached Then the process zone takes place which is where the crack formation takes place with decreasing tensile stress on a crack face due to a bridging effect. Finally, when the stress is completely releases, the crack opening contrinues without any stress, hence the failure (cracked) zone.

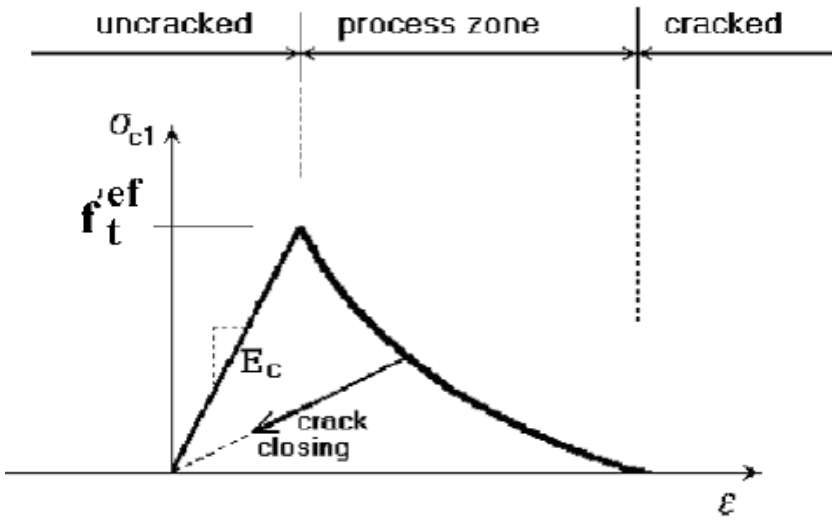

Figure 4-13: Stages of crack opening

The smeared crack approach for modeling of cracks is adopted in the model. Out of the two fixed crack and rotated crack options, the fixed crack approach is adopted here. In this approach the crack direction is given by the principal stress direction at the moment of the crack initiation. During further loading this direction is fixed and represents the material axis of the orthotropy.

The shear modulus is then reduced according to the law derived by Kolmar [24] after cracking. With growing strain normal to the crack, the shear modulus is reduced due to the crack opening.

$$
\begin{aligned}
r_g &= c_3 \frac{-\ln(\frac{1000\varepsilon_u}{c_1})}{c_2} \\
c_1 &= 7 + 333(p - 0.005) \\
c_2 &= 10 - 167(p - 0.005) \\
0 &\le p \le 0.02
\end{aligned}
\qquad \textbf{(4-21)}
$$

Where:

ε_u is strain normal to the crack

c_1 to c_3 are Kolmar coefficients determined based on sample specific parameters in experiments [24]

r_g is the shear retention factor

G is the reduced shear modulus

G_c is the initial concrete shear modulus

p is Kolmar's fracture process zone coefficient

$$G_c = \frac{E_c}{2(1+\nu)} \qquad \textbf{(4-22)}$$

4.2.2 Failure Criterion

The Rankine criterion for concrete cracking is used to set a failure limit in our model. It is assumed that strains and stresses are converted into the material direction which is given by the principal direction at the onset of cracking [12].

4.2.3 Cohesive Crack Model – The Energy Approach

The loading condition we are considering is a monotonic loading and no unloading occurs in the fracture process zone. This allows us to define the process zone boundary by only the crack length a.

Potential energy of the cracked body:

$$\Pi(u_i, P, a) = \int_V W(\varepsilon_{ij})dV - \int_V F_i u_i dV - P\int_{A_T} b_i u_i dA + \int_{A_p} \phi(w)dA \qquad \textbf{(4-23)}$$

W is the strain density function defined in the body

ε_{ij} is the strain field

F_i is the body force

u_i is an admissible displacement field for the system

b_i is the boundary force distribution defined in the part of boundary A_T

ϕ is the potential defined for any given cohesive law $\sigma = f(w)$

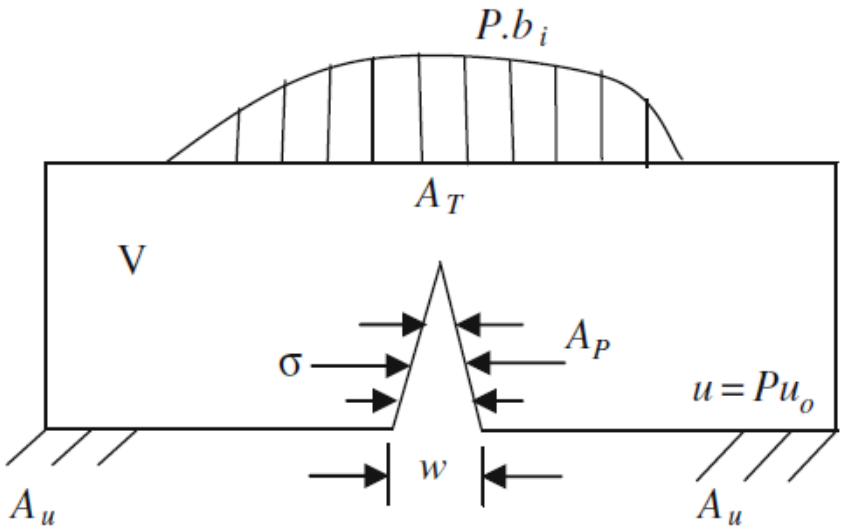

Figure 4-14: Parameters taken into account in potential energy of the cracked body

The displacement equilibrium is then obtained by setting the first order derivation of the potential energy with respect to the displacement to zero.

4.2.4 Softening Function – Bilinear Softening

There are several softening function forwarded by different researchers. The bilinear softening function is adopted in the ATENA model prepared. The bilinear function is expressed as:

$$\sigma = f_t - (f_t - \sigma_s)\frac{w}{w_s},\ for\ 0 \le w \le w_s$$
$$\sigma = \sigma_s \frac{w_c - w}{w_c - w_s},\ for\ w_s \le w \le w_c \qquad \textbf{(4-24)}$$
$$\sigma = 0,\ for\ w_c \le w$$

Where w is

w is actual crack opening width

w_c is maximum crack opening width as per the softening function

w_s is minimum crack opening width as per the softening function

σ is tensile stress at crack tip

σ_c is compressive stress in concrete cross-section

As discussed earlier, the area under the softening curve gives the total fracture energy.

In their book Kumar and Barazi [22] have forwarded the values of the crack opening width for several values of aggregate sizes. The crack opening width is calculated using built in function in the ATENA software that takes into account the manually assigned fracture energy and the tensile strength of the concrete using the following relation:

$$w_c = \frac{3.6G_F}{f_t} \qquad \textbf{(4-25)}$$

Having carried out parametric studies Kumar and Barazi have forwarded the following remarks regarding the cohesive crack fracture approach to finite element modeling of concrete elements and it is worth mentioning here because it affects the concluding remarks in this specific research works. The peak load gained from test results show that the cohesive crack model within about 6% accuracy in the bilinear and nonlinear softening functions.

4.2.5 Iterative Stiffness Reduction

The development of the above stiffness matrix, see equation 1-2 and 1-3, to an end of determining the stress-strain relation for fracture process zone is derived from the condition that the strain of the material between the crack is unrelated to the strain elsewhere except the fact that it is smaller. Furthermore, the stress normal to the cracks must be zero and it is assumed that the material between the cracks behaves as an uncracked elastic material. Even though these assumptions are somewhat unrealistic they are necessary for the analysis approach proposed.

4.2.6 Modeling Cracks

The smeared crack approach for modeling of cracks is adopted in ATENA as mentioned in the second chapter of this document. There are two available options for modeling of cracks within the smeared crack modeling framework. These options are the fixed crack and rotated crack models.

Crack initiation is set when the principal stress exceeds the tensile strength of the concrete in both fixed and rotated crack models. According to the concept of smeared crack approach, cracks are uniformly distributed within the material volume, which is also the same in both approaches.

In fixed crack model, the crack direction is first set by the principal stress direction at the moment of crack initiation. As the loading continues to increase, the direction of the cracks remains unchanged representing the material axis of orthotropy. With the assignment of the orthotropy, the material axis is normal to the crack direction and the strong axis is parallel with the cracks as shown in the figure below:

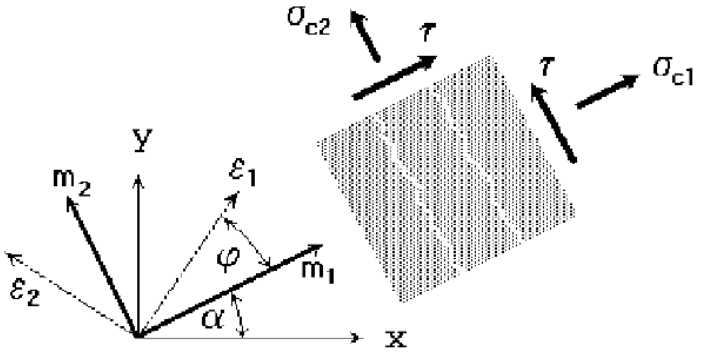

Figure 4-15: Fixed crack modeling approach

On the other hand, the rotated crack model sets the direction of the principal stress to coincide with the direction of the principal strain at each loading step. Thus, no shear strain occurs on the crack plane and only normal stress components are defined.

The direction of the cracks also rotated with the rotation of the principal strain axis. ATENA ensures the co-axiality of the principal strain axes with the material axes by iteratively computing the tangent shear modulus at each loading step using the relation:

$$G_t = \frac{\sigma_{c1} - \sigma_{c2}}{2(\varepsilon_1 - \varepsilon_2)} \qquad \textbf{(4-26)}$$

Figure 4-16 describes the above explained rotating crack approach:

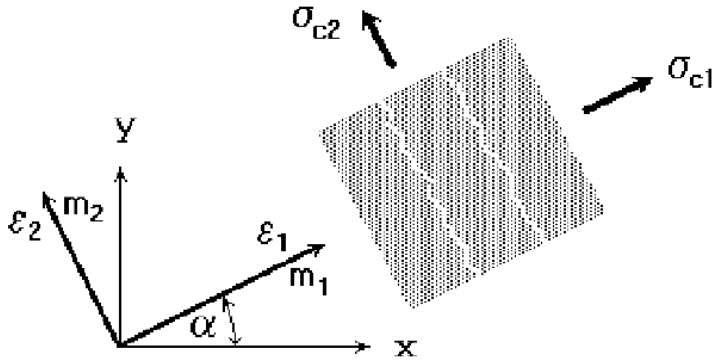

Figure 4-16: Rotated crack modeling approach

From the above two crack modeling alternatives, the fixed crack model has been adopted. This is because in the fixed crack model a strain field rotation generates shear

stress on the crack plane and consequently the model of shear becomes more vivid to analyze as opposed to the rotated crack approach where shear on the crack plane never appears.

4.2.7 Basic Assumptions

The following basic assumptions are considered in the development of the cohesive crack model [24]

- The bulk of material outside the fracture process zone behaves in a linear elastic and isotropic manner
- Concrete is modeled as a homogenous material without taking into account statistical variation in aggregate distribution (Weibull theory discussed in the preceding chapters has not been implemented)
- The cohesive process zone begins to develop when the maximum principal stress becomes equal to the tensile strength.
- The material is in partially damaged condition and is still able to transfer stress known as cohesive stress after formation of cohesive fracture zone.

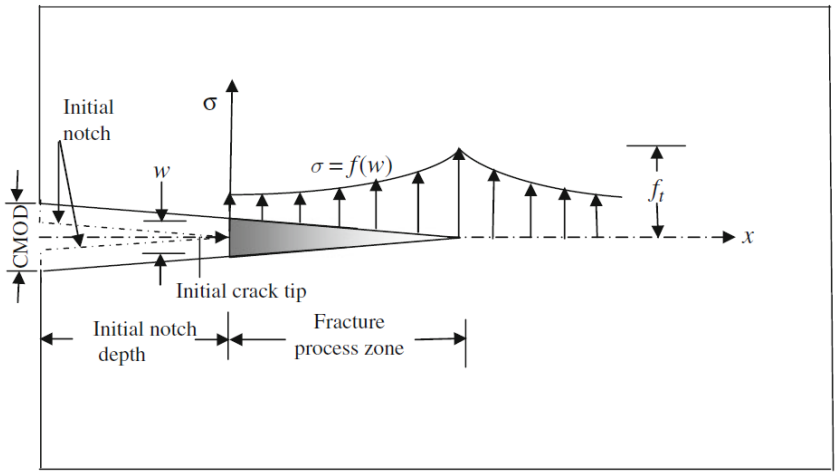

Figure 4-17: Stress Distribution and cohesive stress growth in cracked concrete

The total fracture energy is then mathematically written as:

$G_F = \int_0^{w_c} f(w)dw$ which shows that the fracture energy is directly related with the softening function discussed above.

4.3 Software Verification

Prior to analyzing the main sample beams of this research, the above described modeling basis and the choice of the analysis software itself is put under test for verification. Under this sub-topic ten sample beams whose shear capacities has already been computed in the analytical calculation chapter and that were tested in scientific laboratories were taken and modeled in the above described frame work. The following section presents the software output for these verifying beams:

4.3.1 Verifying beams

4.3.1.1 Verifying beam - 1

The first beam taken for software verification is the experimental beam by Leonhard tested in 1962. It is a simply supported beam spanning 1960mm with two concentrated loads acting symmetrically separated at a distance of 330mm. The beam depth is 320mm and its width is 190mm. Tensile reinforcement of 1060mm^2 is also used. The concrete's cylindrical compressive capacity is 28.5MPa and the reinforcement yield strength is 400MPa.Hence the ATENA model prepared henceforth is strictly as per the specifications described above.

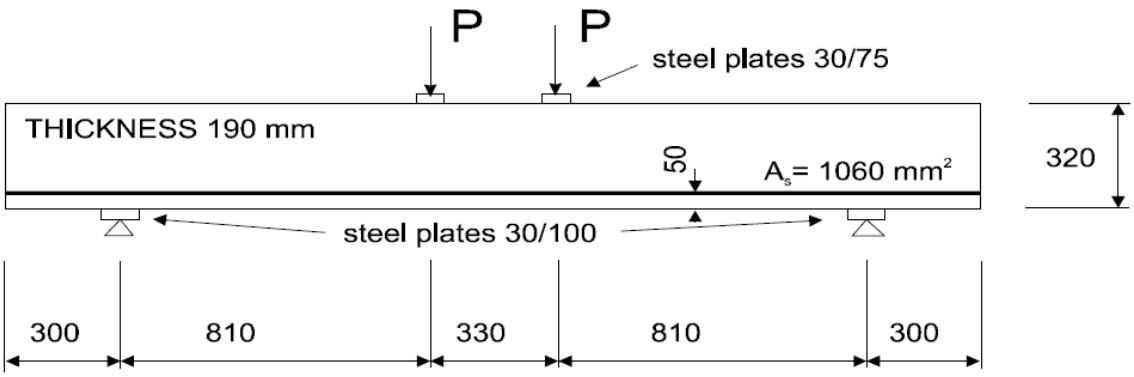

Figure 4-18: Verifying beam 1

According to the compiled data published by Collins [25] the experimental data shows that the beam fails in shear and has a maximum loading recorded to be 96.28kN. Below is shown the ATENA model outputs for this beam according to the specifications shown in the publication by Collins [25].

The software input parameters are not discussed in detail under this chapter because the model basis has been thoroughly discussed in the preceding subtopics. The output for the first verifying beam is shown graphically as follows.

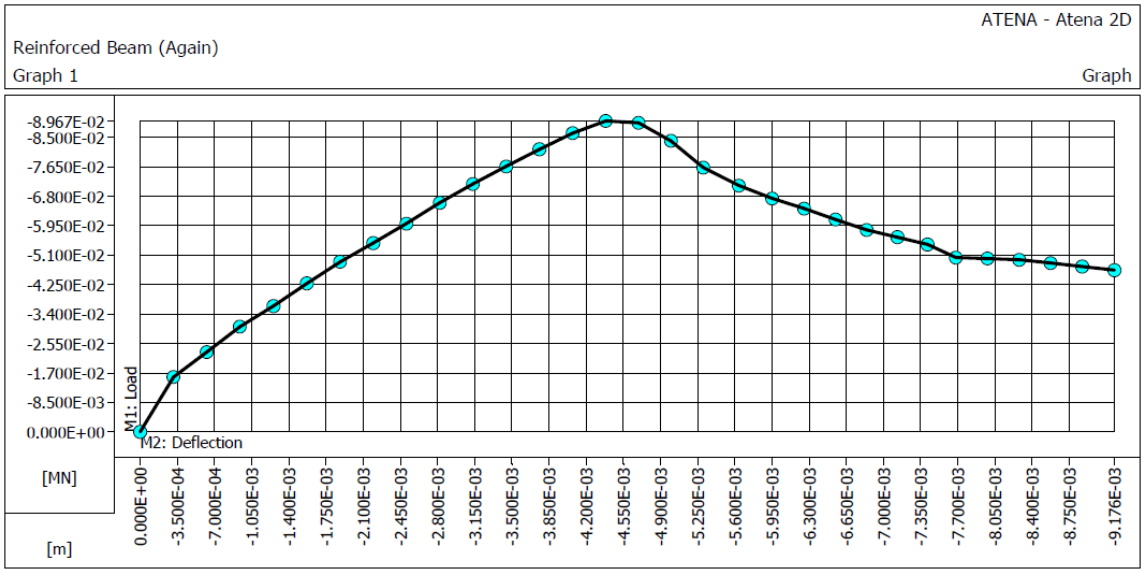

Figure 4-19: ATENA output for Verifying beam 1

As shown in the graphical representation, the maximum load carrying capacity of the beam is 89.67kN. The ATENA model has a 6.8% deviation from the actual laboratory result.

4.3.1.2 Verifying beam – 2

The second beam taken for software verification is the experimental beam by Walraven and Lehwa tested in 1994. All necessary input data about this specific beam is presented in the paper published by Collins [25]. The beam is a simply supported beam spanning 2160mm with single concentrated load acting at its center. The beam depth is 750mm and its width is 200mm. Tensile reinforcement of 1137.6mm^2 was also used in the experiment. The concrete's cylindrical compressive capacity is 23.2MPa and the reinforcement yield strength is 440MPa. Hence, the ATENA model prepared henceforth is strictly as per the specifications described above.

According to the compiled data published by Collins [25] the experimental data shows that the beam fails in shear and carries a maximum load of 226.0kN. Below is shown the ATENA model outputs for this beam according to the specifications shown in the publication by Collins [25].

The ATENA software output for Walraven's beam is shown graphically as follows:

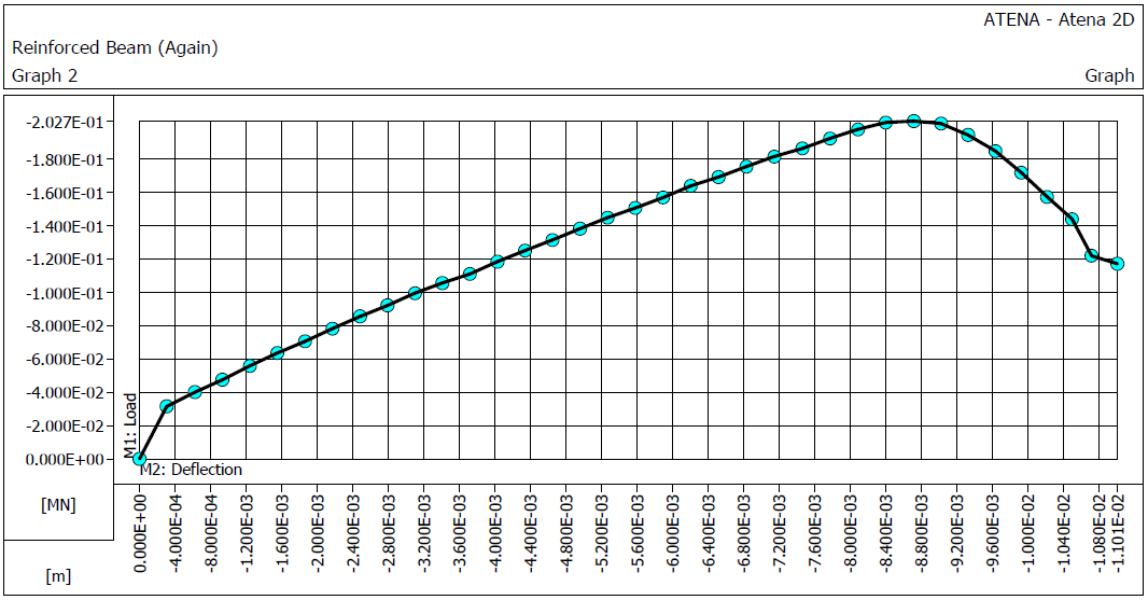

Figure 4-20: ATENA output for verifying beam - 2

As shown in the graphical representation, the maximum load carrying capacity of the beam is 202.7kN. The ATENA model has a 10.3% deviation from the actual laboratory result.

4.3.1.3 Verifying beam – 3

The third beam taken for software verification is the experimental beam by Kani tested in 1969. All necessary input data about this specific beam is presented in the paper published by Collins [25]. Kani's beam is a simply supported beam spanning 3382mm with single concentrated load acting at its center. The beam depth is 1219mm and its width is 154mm. Tensile reinforcement of 4553.1mm^2 was also used in the experiment. The concrete's cylindrical compressive capacity is 27.4MPa and the reinforcement yield strength is 345MPa. Hence, the ATENA model prepared henceforth is strictly as per the specifications described above.

According to the compiled data published by Collins [25] the experimental data shows that the beam fails in shear and has a maximum load of 237kN. Below is shown the ATENA model outputs for this beam according to the specifications shown in the publication by Collins [25].

The ATENA software output for Kani's beam is shown graphically as follows:

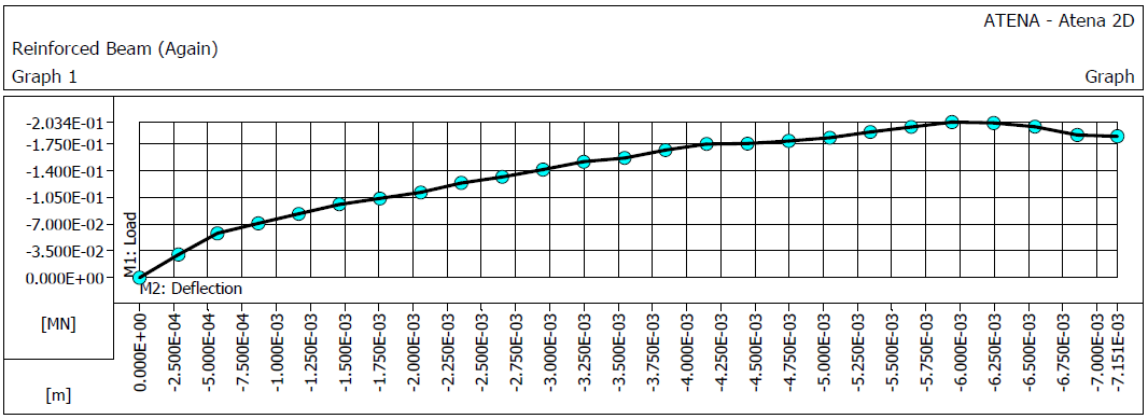

Figure 4-21: ATENA output for verifying beam 3

As shown in the graphical representation, the maximum load carrying capacity of the beam is 203.4kN. The ATENA model has a 11.1% deviation from the actual laboratory result.

4.3.1.4 Verifying beam – 4

The fourth beam taken for software verification is the experimental beam by Collin tested in 2004. All necessary input data about this specific beam is presented in the paper published by Collins [25]. The Toronto beam is a simply supported beam spanning 24000mm with single concentrated load acting at its center. The beam depth is 4000mm and its width is 250mm. Tensile reinforcement of 6329.38mm^2 was also used in the experiment. The concrete's cylindrical compressive capacity is 37MPa and the reinforcement yield strength is 400MPa. Hence, the ATENA model prepared henceforth is strictly as per the specifications described above.

According to the compiled data published by Collins [25] the experimental data shows that the beam fails in shear and has a maximum load of 685kN. Below is shown the ATENA model outputs for this beam according to the specifications shown in the publication by Collins [25].

The ATENA software output for the Toronto beam is shown graphically as follows:

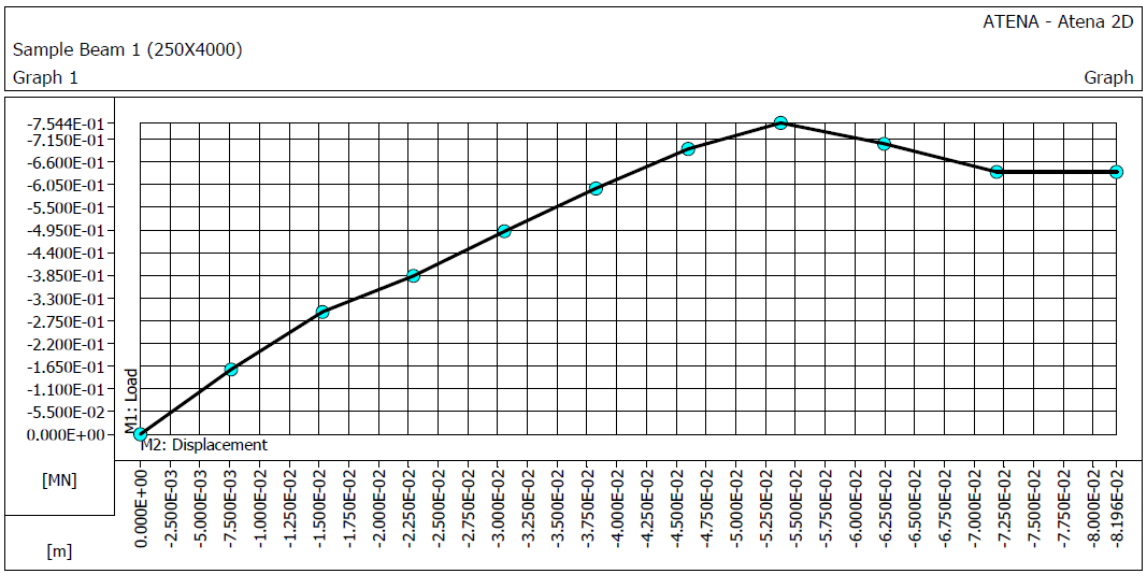

Figure 4-22: ATENA output for verifying beam 4

As shown in the graphical representation, the maximum load carrying capacity of the beam is 754.4kN. The ATENA model has a 10.13% deviation from the actual laboratory result.

4.3.1.5 Verifying beam – 5

The fifth beam taken for software verification is the experimental beam by Regan tested in 1975. All necessary input data about this specific beam is presented in the paper published by Collins [25]. Regan's beam is a simply supported beam spanning 900mm with single concentrated load acting at its center. The beam depth is 100mm and its width is 400mm. Tensile reinforcement of 551.12mm^2 was also used in the experiment. The concrete's cylindrical compressive capacity is 37.8MPa and the reinforcement yield strength is 670MPa. Hence, the ATENA model prepared henceforth is strictly as per the specifications described above.

According to the compiled data published by Collins [25] the experimental data shows that the beam fails in shear and has a maximum load of 62.5kN. Below is shown the ATENA model outputs for this beam according to the specifications shown in the publication by Collins [25].

The ATENA software output for the Toronto beam is shown graphically as follows:

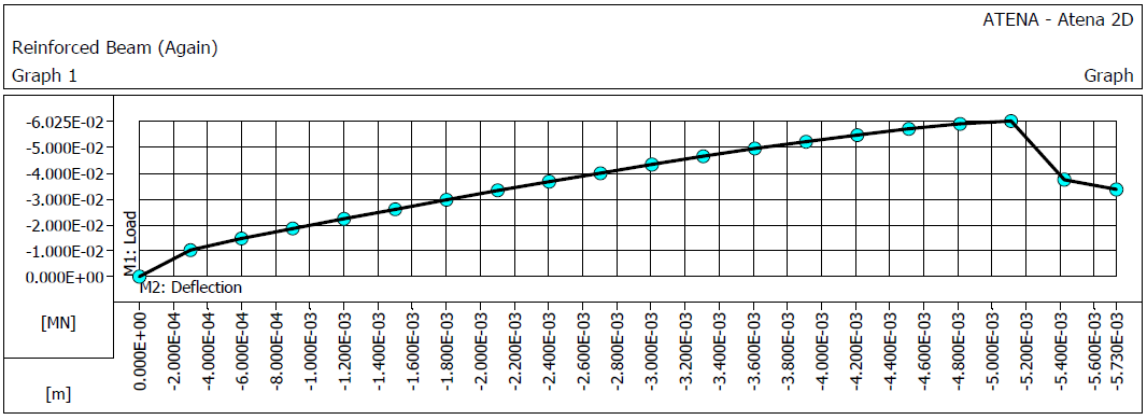

Figure 4-23: ATENA output for verifying beam 5

As shown in the graphical representation, the maximum load carrying capacity of the beam is 60.25kN. The ATENA model has a 3.6% deviation from the actual laboratory result.

4.3.1.6 Verifying beam – 6

The sixth beam taken for software verification is the experimental beam by Batson tested in 1982. All necessary input data about this specific beam is presented in the paper published by Collins [25]. Batson's beam is a simply supported beam spanning 1220mm with single concentrated load acting at its center. The beam depth is 152mm and its width is 102mm. Tensile reinforcement of 401.57mm^2 was also used in the experiment. The concrete's cylindrical compressive capacity is 34.7MPa and the reinforcement yield strength is 276MPa. Hence, the ATENA model prepared henceforth is strictly as per the specifications described above.

According to the compiled data published by Collins [25] the experimental data shows that the beam fails in shear and has a maximum load of 19.2kN. Below is shown the ATENA model outputs for this beam according to the specifications shown in the publication by Collins [25].

The ATENA software output for the Toronto beam is shown graphically as follows:

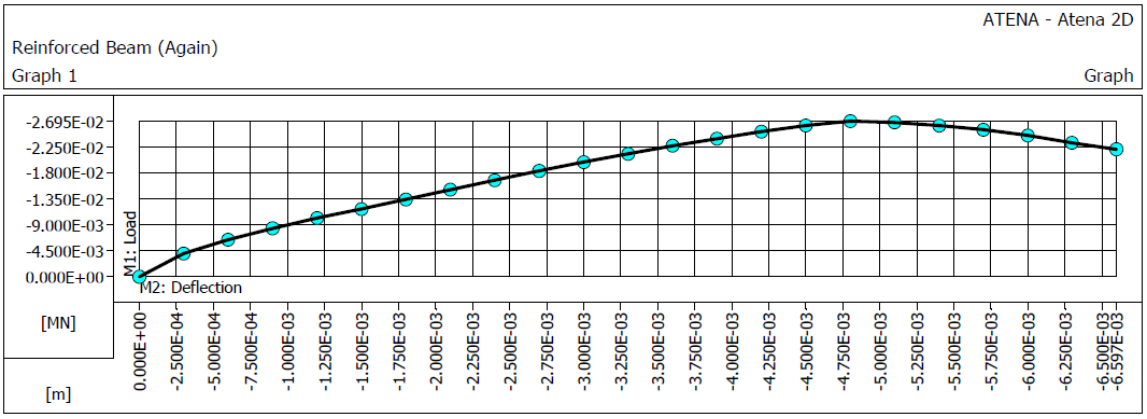

Figure 4-24: ATENA output for verifying beam 6

As shown in the graphical representation, the maximum load carrying capacity of the beam is 26.95kN. The ATENA model has a 40.36% deviation from the actual laboratory result.

4.3.1.7 Verifying beam – 7

The seventh beam taken for software verification is the experimental beam by Taylor tested in 1990. All necessary input data about this specific beam is presented in the paper published by Collins [25]. Batson's beam is a simply supported beam spanning 5600mm with single concentrated load acting at its center. The beam depth is 1000mm and its width is 400mm. Tensile reinforcement of 5022mm^2 was also used in the experiment. The concrete's cylindrical compressive capacity is 28.7MPa and the reinforcement yield strength is 420MPa. Hence, the ATENA model prepared henceforth is strictly as per the specifications described above.

According to the compiled data published by Collins [25] the experimental data shows that the beam fails in shear and has a maximum load of 358.4kN. Below is shown the ATENA model outputs for this beam according to the specifications shown in the publication by Collins [25].

The ATENA software output for the Toronto beam is shown graphically as follows:

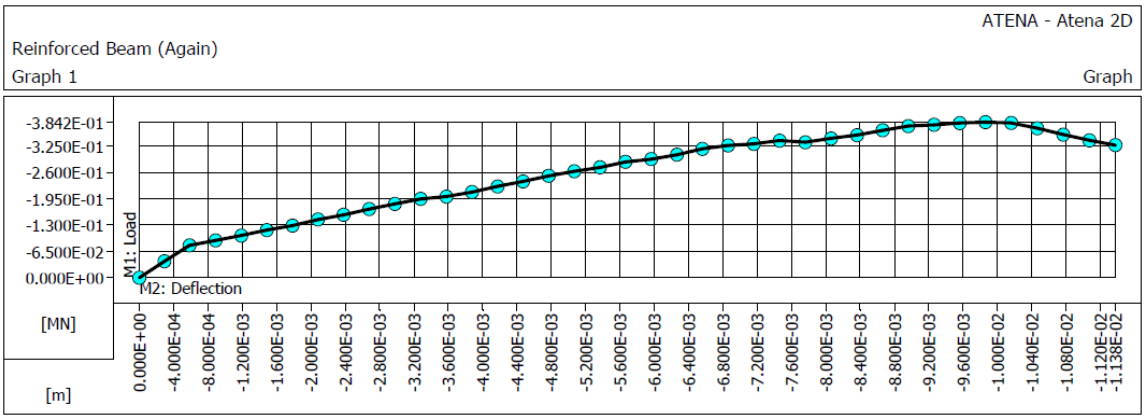

Figure 4-25: ATENA output for verifying beam 7

As shown in the graphical representation, the maximum load carrying capacity of the beam is 384.2kN. The ATENA model has a 7.1% deviation from the actual laboratory result.

4.3.1.8 Verifying beam – 8

The eighth beam taken for software verification is the experimental beam by Niwa tested in 1969. All necessary input data about this specific beam is presented in the paper published by Collins [25]. Niwa's beam is a simply supported beam spanning 12000mm with single concentrated load acting at its center. The beam depth is 2100mm and its width is 600mm. Tensile reinforcement of 3360mm^2 was also used in the experiment. The concrete's cylindrical compressive capacity is 27.1MPa and the reinforcement yield strength is 999MPa. Hence, the ATENA model prepared henceforth is strictly as per the specifications described above.

According to the compiled data published by Collins [25] the experimental data shows that the beam fails in shear and has a maximum load of 402kN. Below is shown the ATENA model outputs for this beam according to the specifications shown in the publication by Collins [25].

The ATENA software output for the Toronto beam is shown graphically as follows:

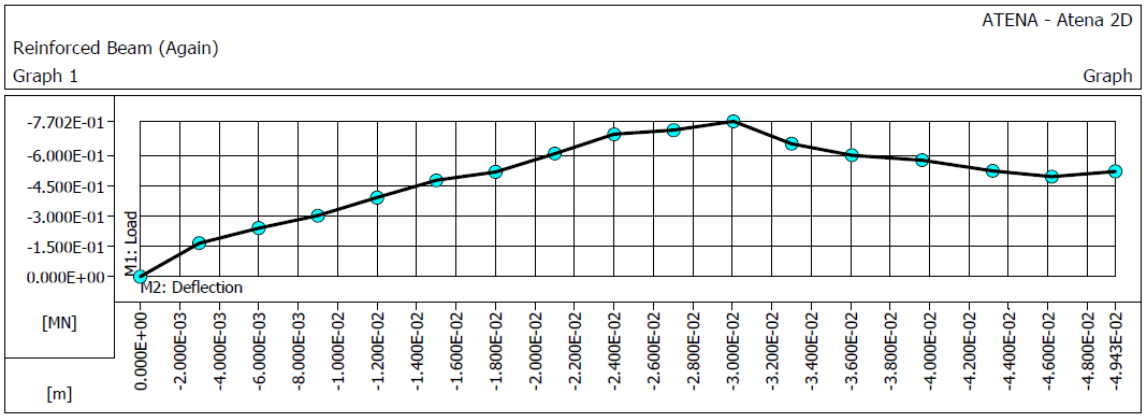

Figure 4-26: ATENA output for verifying beam 8

As shown in the graphical representation, the maximum load carrying capacity of the beam is 770.2kN. The ATENA model has a 91.5% deviation from the actual laboratory result.

4.3.1.9 Verifying beam – 9

The ninth beam taken for software verification is the experimental beam by Johnson tested in 1998. All necessary input data about this specific beam is presented in the paper published by Collins [25]. Johnson's beam is a simply supported beam spanning 3340mm with single concentrated load acting at its center. The beam depth is 610mm and its width is 305mm. Tensile reinforcement of 409.34mm^2 was also used in the experiment. The concrete's cylindrical compressive capacity is 55.9MPa and the reinforcement yield strength is 525MPa. Hence, the ATENA model prepared henceforth is strictly as per the specifications described above.

According to the compiled data published by Collins [25] the experimental data shows that the beam fails in shear and has a maximum load of 191.5kN. Below is shown the ATENA model outputs for this beam according to the specifications shown in the publication by Collins [25].

The ATENA software output for the Toronto beam is shown graphically as follows:

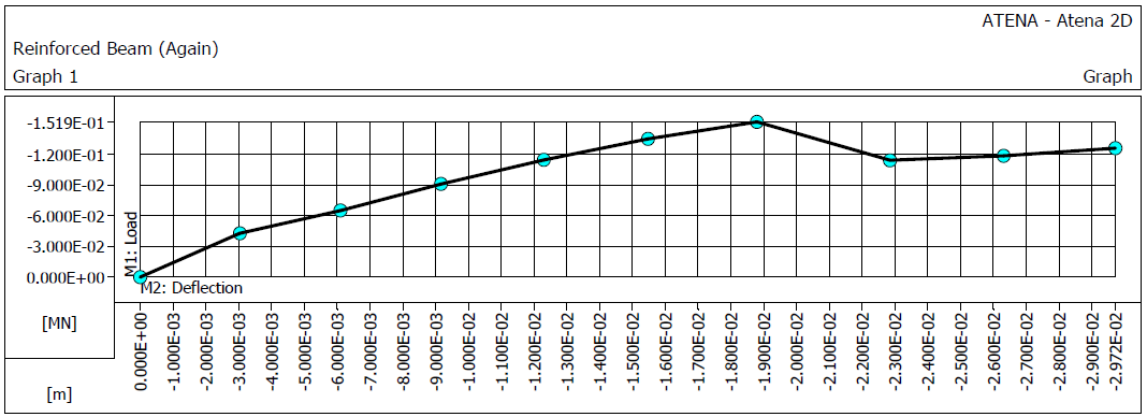

Figure 4-27: ATENA output for verifying beam 9

As shown in the graphical representation, the maximum load carrying capacity of the beam is 151.9kN. The ATENA model has a 20.68% deviation from the actual laboratory result.

4.3.1.10 Verifying beam – 10

The tenth beam taken for software verification is the experimental beam by Kawano tested in 1973. All necessary input data about this specific beam is presented in the paper published by Collins [25]. Kawano's beam is a simply supported beam spanning 12000mm with single concentrated load acting at its center. The beam depth is 2200mm and its width is 600mm. Tensile reinforcement of 14400mm^2 was also used in the experiment. The concrete's cylindrical compressive capacity is 23.1MPa and the reinforcement yield strength is 400MPa. Hence, the ATENA model prepared henceforth is strictly as per the specifications described above.

According to the compiled data published by Collins [25] the experimental data shows that the beam fails in shear and has a maximum load of 560kN. Below is shown the ATENA model outputs for this beam according to the specifications shown in the publication by Collins [25].

The ATENA software output for the Toronto beam is shown graphically as follows:

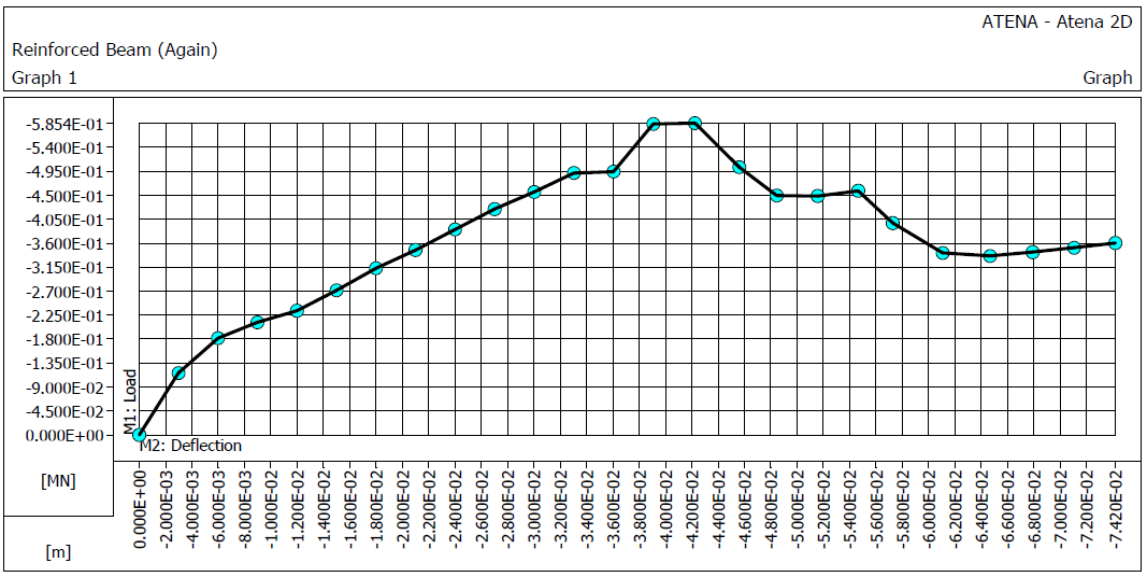

Figure 4-28: ATENA output for verifying beam 10

As shown in the graphical representation, the maximum load carrying capacity of the beam is 585.4kN. The ATENA model has a 4.53% deviation from the actual laboratory result.

4.3.2 Summary of Software Verification

The table below presents a summary of the software verification procedure discussed in the preceeding sub-topic.

Table 4-10: Summary of software verification

Beam ID	ATENA prediction (kN)	Experimental Finding (kN)	Percentage Error
V-Beam 1	89.67	96.28	6.87%
V-Beam 2	202.7	226	10.31%
V-Beam 3	203.4	237	14.18%
V-Beam 4	754.4	685	-10.13%
V-Beam 5	60.25	62.5	3.60%
V-Beam 6	26.95	19.2	-40.36%
V-Beam 7	384.2	358.4	-7.20%
V-Beam 8	770.2	402	-91.59%
V-Beam 9	151.9	191.5	20.68%
V-Beam 10	585.4	560	-4.54%

The detail discussion of the analysis results is presented in the discussion of results subtopic. With the exception of 3 beams the shear capacity of the verifying beams us predicted with a percentage error below 15%. This validates the use of the software for the main sample beams picked for this specific research.

Having set that the software is applicable for shear capacity prediction, the analysis procedure for the actual sample beams is discussed hereafter.

4.4 Sample Beam Models and Results

4.4.1 Geometry

Due to the limitation in the availability of the complete version of the ATENA software, The ATENA demo version has been used for this research. The major limitation in the demo version is the limit on the number of nodes that is allowed for the analysis procedure. The number of nodes that is allowed in this version is only 300. Hence, it was important to find a means to lower the number of nodes that is necessary in order to obtain an accurate analysis output.

It is to this end that the simply supported beams with variable depths ranging from 2m to 4m are modeled. These beams span 24m as discussed in the modeling basis subtopic. However, they are modeled as 12m beams by taking advantage of the symmetry at their mid-span.

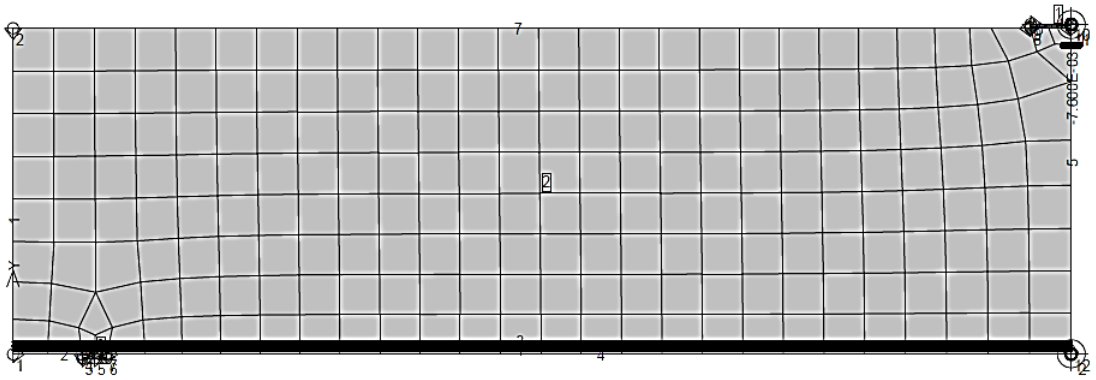

Figure 4-29: FEM Model of one of the Sample beams

4.4.2 Material Property

There are three types of materials used in the finite element model. These include, reinforcement bar, concrete and steel plate

4.4.2.1 Concrete

Elastic modulus = 3.403E+04 [MPa]

Poisson's ratio = 0.200 [-]

Tensile strength = 2.807E+00 [MPa]

Compressive strength = -3.200E+01 [MPa]

Type of tension softening: Bilinear

Specific fracture energy = 7.018E-05 [MN/m]

Crack model: Fixed

Reduction of compressive strength due to cracks = 0.800 [-]

Type of compression softening: Crush Band

Critical compressive displacement = -5.0000E-04 [m]

Shear Retention Factor: Variable

Tension-compression interaction: Linear

Specific material weight Rho = 2.300E-02 [MN/m^3]

Coefficient of thermal expansion Alpha = 1.200E-05 [1/K]

4.4.2.2 Reinforcement

Type: Linear

Elastic modulus = 2.000E+05 [MPa]

Specific material weight = 7.850E-02 [MN/m3]

Coefficient of thermal expansion = 1.200E-05 [1/K]

Active in compression

4.4.2.3 Steel Plate

Elastic modulus = 2.000E+05 [MPa]

Poisson's ratio = 0.300 [-]

Specific material weight Rho = 2.300E-02 [MN/m3]

Coefficient of thermal expansion Alpha = 1.200E-05 [1/K]

The adoption of a steel plate is to provide a platform for loading and restraint application point. This is generally to avoid a crushing failure at or near to the node where such actions are applied.

4.4.3 Loading and restraint

The main interest of the research is to determine the load carrying capacity of the member. This implies that the structures response in the post-peak regime is also important. For that reason, the loading on the beam is applied by prescribed displacement at the top of the steel plate. This displacement value is then gradually increased in each load step and the performance of the structure is analyzed at these loading steps.

The loading history works in a similar manner as other similar finite element software, the first load cases are defined, and they are combined together to form a loading history for the structure under study.

A vertical direction constraint is applied at the other end of the truncated beam to take into account the restraint. As discussed in the previous chapter, the beam is simply supported beam and hence no further restraint is added at this point.

Due to the simplification of truncation introduced, the beam is provided with a horizontal direction restrain at the axis of symmetry.

Below is presented a summary of the two load cases used to define the above mentioned restraint and loadings:

Load case 1

Properties

Name: Load case with supports

Coefficient: 1.0000 [-]

Code: Supports Joint support

X direction support

Y direction support

Line name: 5

Fixed Global

Load case: 2

Properties

Name: Load case with actions

Coefficient: 1.0000 [-]

Code: Prescribed deformation

Joint deformation

Joint: Support and deformation

Fixed: -7.600E-03 Global

4.4.4 Monitoring Points

To observe the structure response at every step of the analysis, two monitoring points are used in the finite element model. The first monitoring point is located at the point of load application. This monitoring point helps to keep track of the loading increment at each analysis step. The other monitoring point used is located at the bottom center of the non-truncated beam. This point is used to record the exhibited deflection in the member which will then enable us to study the loading and deformation relations when combined with the first monitoring point.

4.4.5 Analysis outputs

4.4.5.1 Sample Beam 1 – 250mmX4000mm

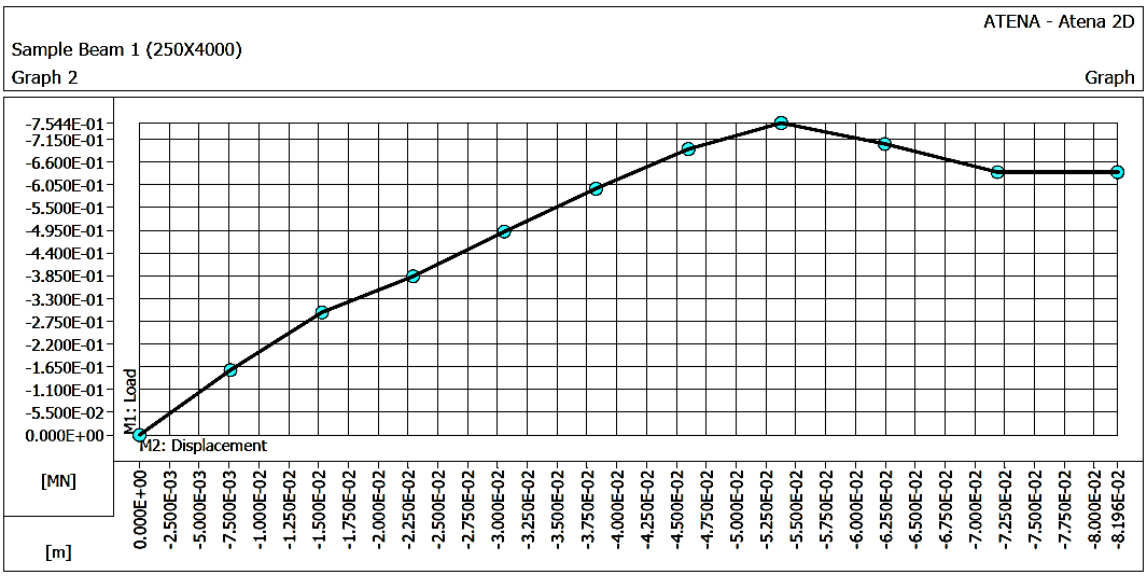

Figure 4-30: Load - deformation diagram for sample beam – 1

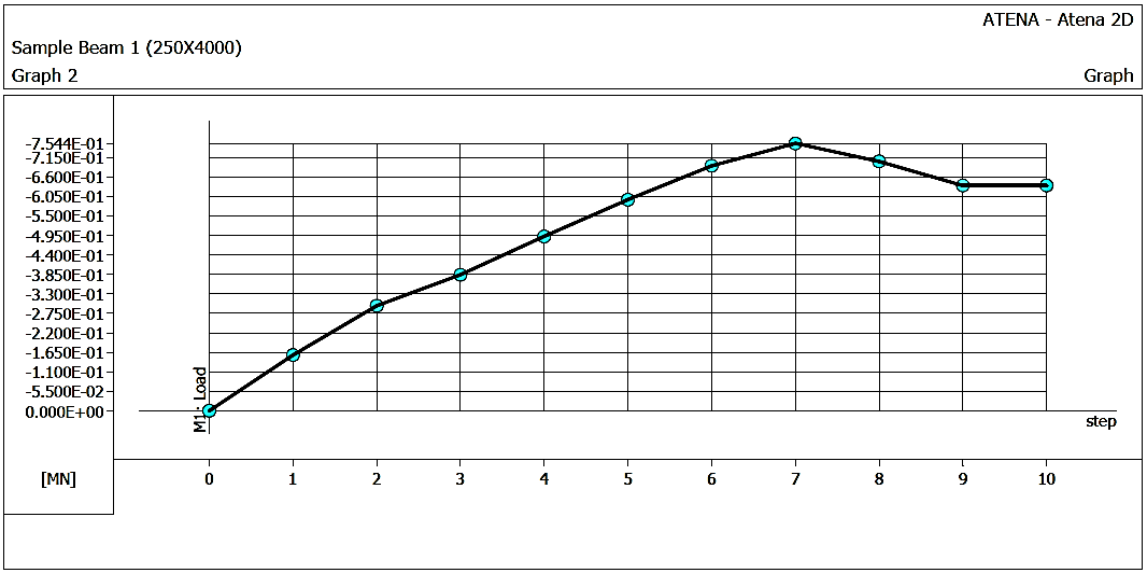

Figure 4-31: Load - analysis step diagram for sample beam -1

4.4.5.2 Sample Beam 2 – 250mmX3500mm

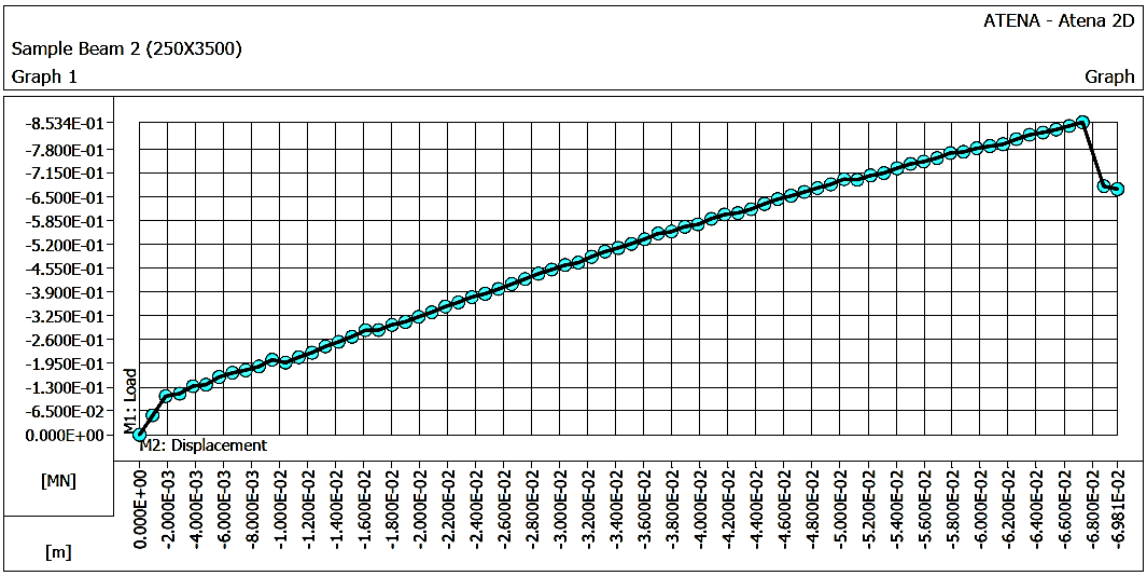

Figure 4-32: Load - deformation diagram for sample beam -2

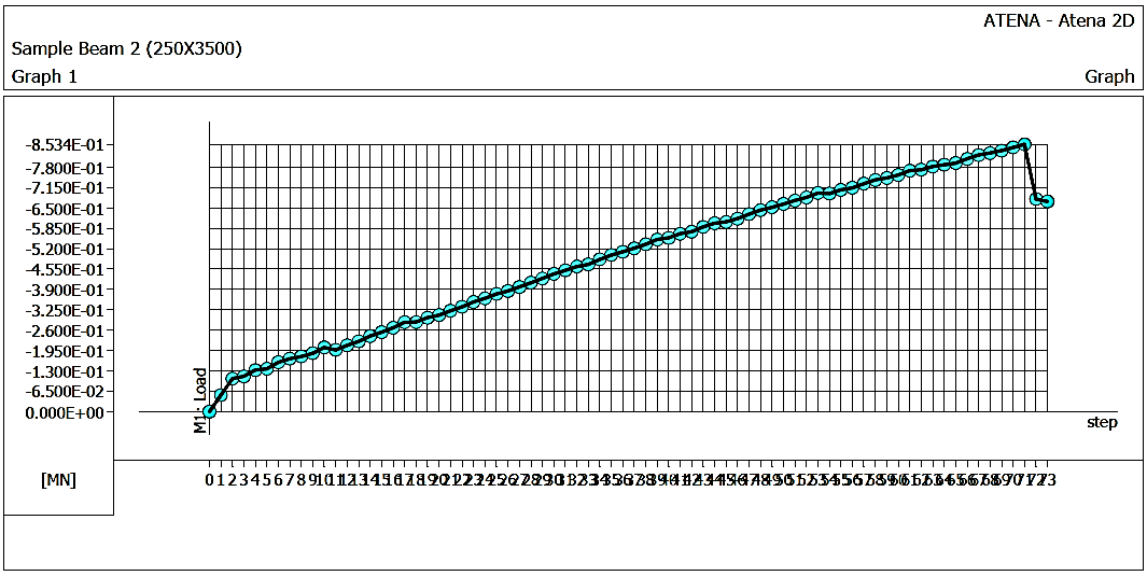

Figure 4-33: Load - analysis step diagram for sample beam – 2

4.4.5.3 Sample Beam 3 – 250mmX3000mm

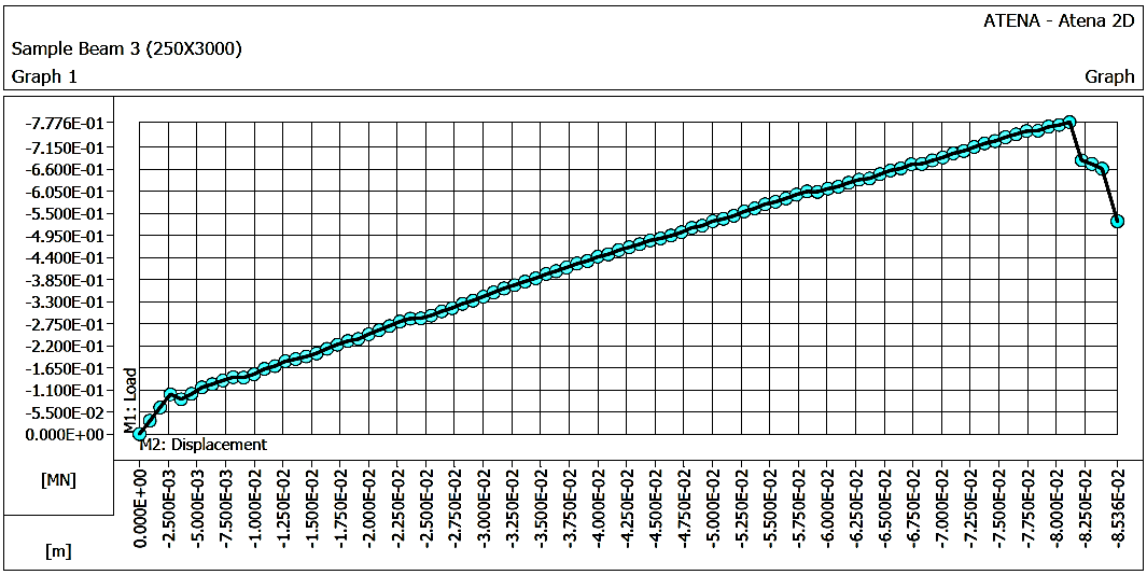

Figure 4-34: Load - deformation diagram for sample beam – 3

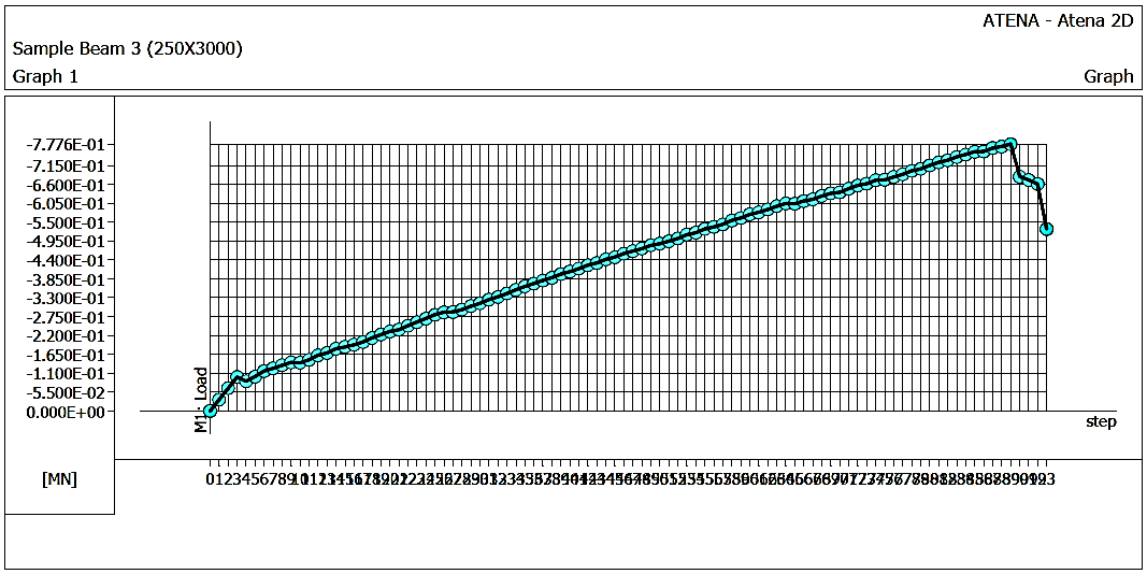

Figure 4-35: Load - analysis step diagram for sample beam – 3

4.4.5.4 Sample Beam 4 – 250mmX2500mm

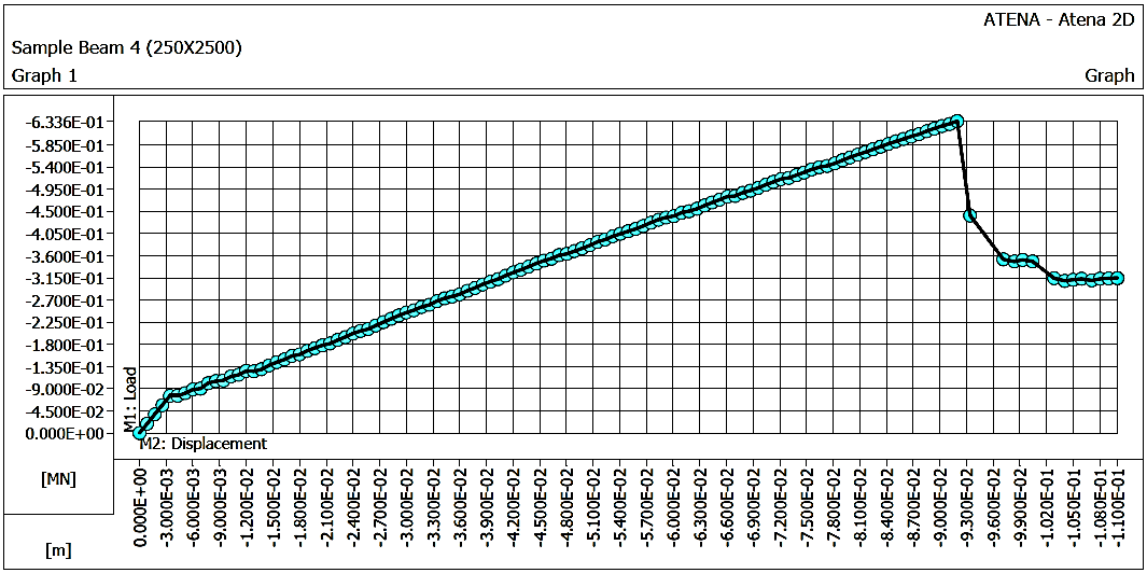

Figure 4-36: Load - deformation diagram for sample beam - 4

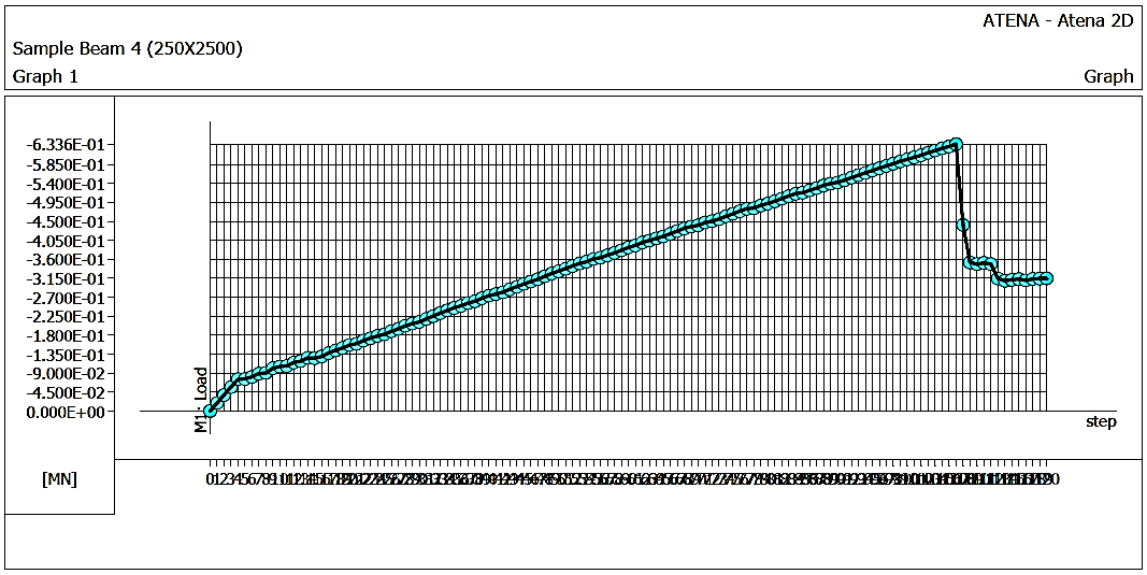

Figure 4-37: Load - analysis step diagram for sample beam – 4

4.4.5.5 Sample Beam 5 – 250mmX2000mm

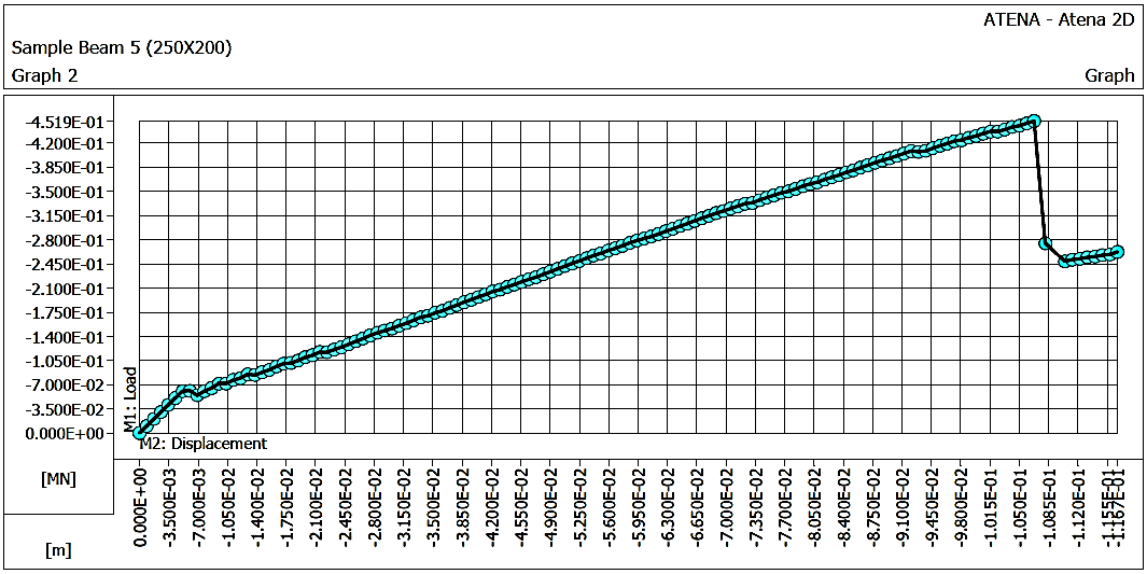

Figure 4-38: Load - deformation diagram for sample beam – 5

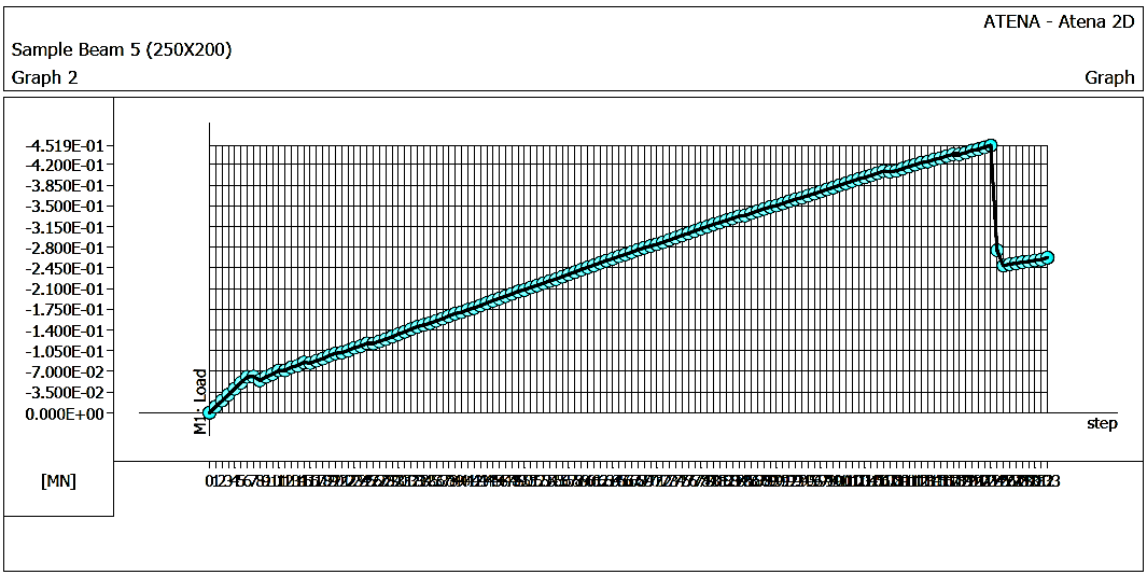

Figure 4-39: Load - analysis step diagram for sample beam - 5

Discussion of results

The incorporation of size effect in predicting the shear capacity of reinforced concrete beams is the main initiation for this research. Despite the wide usage of the two sample building codes taken for overlook in this research, the reduction in shear capacity of the sample beams with-increment in depth is not observed.

The adoption of the fracture mechanics theory based model has proved to solve the lack of size effect incorporation in these codes. The largest beams size, the first sample beam for this study is shown to carry less amount of load that its lower depth counterpart.

In addition to the effect of size in load carrying capacity, the estimation of the two building codes shows a wide gap. Even though this research is not aimed in trying to explain the reason behind this, it can be readily seen that there lacks conclusiveness in the stress based approach, especially as the size of the member increases.

The reference experimental result for the first sample beams proves that the fracture mechanics based approach better predicts member capacities.

Table 4-11: Summary of Results of Shear Capacity Estimation

Beam Label	Cross-section	Bazant's Equation	ES EN Prediction	ACI Prediction	ATENA Prediction	Experimental result
Beam - 1	250mmX4000mm	619.4kN	425.3kN	1022.7kN	754.4kN	685kN
Beam - 2	250mmX3500mm	592.8kN	393.2kN	891.5kN	853.4kN	-
Beam - 3	250mmX3000mm	560.1kN	359.3kN	760.2kN	777.6kN	-
Beam - 4	250mmX2500mm	529.3kN	323.2kN	628.9kN	633.6kN	-
Beam - 5	250mmX2000mm	484.2kN	284.2kN	497.6kN	451.9kN	-

In the diagram below, it can be seen that the ES EN 1992:2015 gives a lower prediction in all depth ranges under study. Further analysis shows its prediction goes higher than the ACI code at lower beam depths. The "size effect" factor in the shear capacity prediction formula falls under question due to such prediction results at larger beam sizes.

The ACI code gives a matching result with the fracture mechanics based approach despite the lack of predicting the inverse effect of the beam size at the larger beam depths under study.

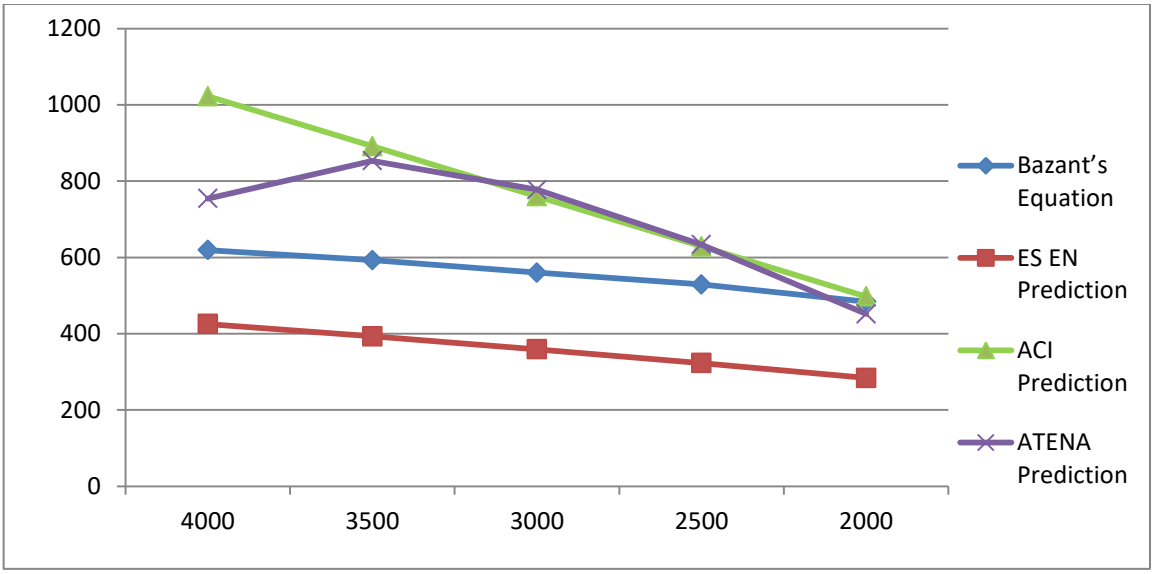

Figure 4-40: Finite element model analysis comparison with code based predictions

It is also important to bring back the analysis outputs for the ten verifying beams discussed previously.

Table 12: Summary of Results of Shear Capacity Estimation for Verifying Beams

Beam ID	Bazant's eqn. prediction (kN)	ES - EN prediction (kN)	ACI prediction (kN)	ATENA prediction (kN)	Experimental Finding (kN)
V-Beam 1	93.87	45.47	47.67	89.67	96.28
V-Beam 2	228.8	69.57	115.59	202.7	226
V-Beam 3	243.6	119.76	143.88	203.4	237
V-Beam 4	609.9	414.8	983.6	754.4	685
V-Beam 5	36.212	31.6	33.9	60.25	62.5
V-Beam 6	12.674	14.78	12.67	26.95	19.2
V-Beam 7	350.65	221.11	330.97	384.2	358.4
V-Beam 8	443.59	372.47	1037.4	770.2	402
V-Beam 9	100.3	87.82	204.12	151.9	191.5
V-Beam 10	506.1	573.65	957.84	585.4	560

Table 13: Percentage Errors in Prediction Methodologies

Beam ID	Bazant's eqn. prediction Percentage Error	ES - EN prediction Percentage Error	ACI prediction Percentage Error	ATENA prediction Percentage Error
V-Beam 1	2.51%	52.78%	50.49%	6.87%
V-Beam 2	-1.23%	69.22%	48.86%	10.31%
V-Beam 3	-2.78%	49.47%	39.3%	14.18%
V-Beam 4	10.97%	39.45%	-43.59%	-10.13%
V-Beam 5	42.07%	49.44%	45.76%	3.6%
V-Beam 6	33.99%	23.03%	34.02%	-40.36%
V-Beam 7	2.17%	38.31%	7.66%	-7.19%
V-Beam 8	-10.34%	7.35%	-158.05%	-91.59%
V-Beam 9	47.63%	54.15%	-6.59%	20.68%
V-Beam 10	9.63%	-2.43%	-71.04%	-4.53%

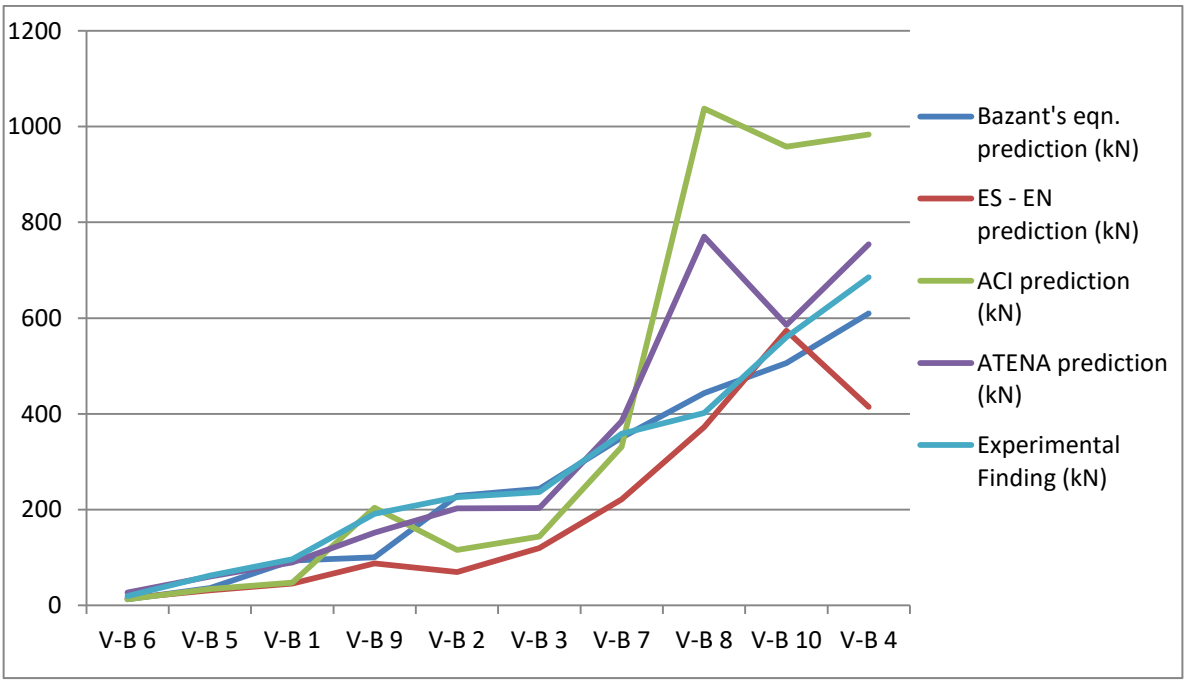

Figure 4-41: Comparison of Shear Capacity Estimation for the Verifying Beams

In summary, the fracture mechanics based approach for the prediction of shear capacity of reinforced concrete beams without shear reinforcement better incorporates the inverse size effect and by far matches experimental results for relatively large beams.

CHAPTER 5 CONCLUSION AND RECOMMENDATION

5.1 Conclusion

From the fracture-mechanics based approach for beam shear capacity estimation and with the comparison made between the two sample building codes and the size effect based formulation forwarded by Bazant [21], the following conclusions are drawn:

- The fracture mechanics based approach takes the size effect into account with better accuracy than the code based approach in the estimation of shear capacity of the sample beams. The fracture mechanics based approach predicts the shear capacity of the sample beams by 37.9% more accurately than the ES EN based approach and 33.9% more accurately than the ACI based approach.
- The shear capacity estimation formula in the simplified approach of the ACI code does not incorporate the size effect on the shear capacity estimation of reinforced concrete beams and hence leads to a 51% overestimation in the shear capacity prediction of the sample beams.
- The factor that takes the size effect into account in ES EN 1992:2015 for shear capacity estimation of reinforced concrete members leads to an underestimation of the actual shear capacity of the sample beams by 38.5% according to the findings of this research.
- The lack of fracture mechanics based approach in the building codes studied results in failure to accurately estimate reinforced concrete beam shear capacity estimations, specifically for large beams.
- The prediction power of non-linear fracture mechanics in shear capacity of concrete beams together with its scientifically plausible energy based approach makes it compelling for adoption into building codes and this research's conclusion adds to many other research conducted in the area with similar remarks.

5.2 Recommendation

- Different parameters including fracture energy, tensile strength of concrete and tensile reinforcement should be used as variables in order to study the effect of each in the prediction power of fracture mechanics based approaches.
- The effect of shear reinforcement in the fracture mechanics based approach shall be studied to better incorporate ductile nature of structural members in failure predictions.
- More research should be conducted on how to include the fracture mechanics based approach in building codes through a simplified mathematical approach that is suitable for design engineers.

REFERENCES

1. Zdenek P. Bazant and Jaime Planas, Fracture and Size Effect in Concrete and Other Quasi-brittle Materials, CRC Press, Boca Raton, Boston, London, New York, Washington D C, 1983

2. James K. Wight and James G. MacGregor, Reinforced Concrete Mechanics and Design, Sixth Edition, Pearson Prentice Hall Publishers, 2009

3. Zdenek P. Bazant and Jin-Keun Kim, 1988, Size Effect in Shear Failure of Longitudinally Reinforced Beams, Journal of Structural Engineering (ASCE), 115(7) pp 1599-1615

4. Vladmir Cervenka, Jan Cervenka, Radomir Pukl, Terezza Sajdloca, Prediction of Shear Failure of Large Beam based on Fracture Mechanics, , Cervenka Consulting, 9th International Conference on Fracture Mechancis of Concrete and Concrete Structures, 2019

5. David Roylance, Introduction to Fracture Mechanics, Departement of Materials Science and Engineering, Masachusetts Institute of Technology, Cambridge, MA., 2001

6. Alberto Carpinteri, 2005, Applications of Fracture Mechanics to Reinforced Concrete, Department of Structural Engineering, 1st edn. Prentice-Hall Inc, Politecnico di Torino, Italy, 2005

7. R Eligehausen and J Ozbolt, Size effect in concrete structures, 1st edn. Prentice-Hall Inc, Politecnico di Torino, Italy, 1990

8. Arne Hillerborg, Shear Strength of Reinfroced Concrete Beams, Division of Building Materials, Lund Institute of Technology, Sweden, Palm Springs publisher, 2005

9. Gustafsson, P. J., Fracture mechanics studies of non-yielding materials like concrete, Division of Building Materials, Lund Institute of Technology, Sweden, Palm Springs publisher, 1985

10. George C. Sih and A. DiTommaso (Editors), Fracture mechanics of concrete: Structural application and numerical calculation, 1985

11. A. Carpinteri, Scale effects in fracture of plain and reinforced concrete structures, 1984

12. S. P. Shah and A. Carpinteri, Fracture Mechanics Test Methods for Concrete, Report of Technical Committee 9-FMT, 2007

13. Vladmir Cervenka, Jan Cervenka, and Radomir Pukl, ATENA – A tool for engineering analysis of fracture in concrete, ACI Journal, 70(12) 788-92 ,2002

14. Vladmir Cervenka, Jan Cervenka, Radomir Pukl, Terezza Sajdloca, Uncertainty of predicting shear strength, ACI Journal, 70(12) 812-95, 2017

15. Vladmir Cervenka, Jan Cervenka, Radomir Pukl, Terezza Sajdloca, Prediction of shear failure of large beams based on fracture mechanics, 2017

16. Walraven, K., Mode Code - Final draft, Volume 1, 2010

17. R. Park and T. Paulay, Reinforced Concrete Structures, Department of Civil Engineering, University of Canterbury, Christchurch, New Zealand, A Wiley-Interscience Publication, 1975

18. Collins, M.P., challenge of Predicting the Shear Strength of Very Thick Slabs, Concrete International V.37 No.11 Nov. 2015, pp 29-37

19. Zdenek P Bazant, Byund Hwan Oh, Crack Band Theory for Fracture of Concrete, Materials and Structures 16:155-177, 1983

20. Zdenek P Bazant, Qiang Yu, Designing Against Size Effect On Shear Strength of Reinforced Concrete Beams Without Stirrups: I. Formulation, Journal of Structural Engineering, 2005, Vol 131, Issue 12 PP. 1877-1885

21. Vahid Broujerdian, Hosseid Kaimpour, Sobhan Alavika, Prediction the Shear Behavior of Reinforced Concrete Beams Using Non-linear Fracture Mechanics, 1999

22. M. T. Kazemi and V. Broujerdian, Reinforced Concrete Beams without Stirrups: Considering shear friction and fracture mechanics, 2002

23. Shailendra Kumar and Sudhirkumar V Barai, Concrete Fracture Models and Application, Springer, New York, 2010

24. Vladmir Cervenka, Libor Jendele and Jan Cervenka, ATENA Program Documentation, Part 1, Prague, 2020

25. Michael P. Collins, Evan C. Bentz and Edward G. Sherwood, Where is Shear Reinforcement Required? A Review of Research Results and Design Procedures, Appendix to ACI Paper, 2008

APPENDIX A

Analytical Calculation based on Bazant's Equation, ES EN 1992:2015 and ACI 318

BAZANT'S EQUATION

Beam - 2

For the second sample beam, Beam – 2 the shear capacity is determined as follows as per the simplified formula given by Bazant and his team [20].

$$V_{Rd,c} = [0.2\rho^{3/8}(1+d/a)\sqrt{f_c'}(1+d/d_o)^{-1/2}]b_w d$$

$$d_o = 694\sqrt{d_a}\,(f_c')^{-2/3}$$

Where:

$$f_c' = 40MPa$$

$d = D - x$; where x is the distance to tensile reinforcement centroid measured from the bottom of the beam cross section.

Assuming there are 3 bars in each layer and there is a clear distance of 30mm between the layers of the reinforcement and also assuming a reinforcement cover of 30mm.

$$x = \frac{3*(30+\frac{30}{2})+3*(30+30+30+\frac{30}{2})+3*(30+30+30+30+30+\frac{30}{2})}{9}$$

$$x = \frac{135+315+495}{9}$$

$$x = 105mm$$

Therefore;

$$d = D - x$$
$$d = 3500mm - 105mm$$
$$d = 3395mm$$

$$a = 12,000mm$$

$$\rho_l = \frac{A_{sl}}{b_W d} \le 0.02$$

$A_{sl} = 9 * \frac{\pi * 30^2}{4} = 6361.73 mm^2$ is the area of the tensile reinforcement

$$\rho_l = \frac{A_{sl}}{b_W d} \le 0.02$$
$$\rho_l = \frac{6361.73}{250 * 3395} = 7.495 * 10^{-3}$$

$b_W = 250 mm$

$\sigma_{cp} = 0$

$d_o = 694\sqrt{d_a}\left(f_c'\right)^{-2/3}$

$d_a = 20 mm$

$d_o = 694\sqrt{20}\left(40\right)^{-2/3}$
$d_o = 265.36$

$V_{Rd,c} = [0.2\rho^{3/8}(1 + d/a)\sqrt{f_c'}(1 + d/d_o)^{-1/2}]b_W d$
$V_{Rd,c} = [0.2(7.495 * 10^{-3})^{3/8}(1 + 3395/12000)\sqrt{40}(1 + 3395/265.36)^{-1/2}] * 250 * 3395$
$V_{Rd,c} = [0.2(0.16)(1 + 0.283) * \sqrt{40} * (1 + 12.794)^{-1/2}] * 848,750$
$V_{Rd,c} = [0.2(0.16)(1.283) * \sqrt{40} * 0.269] * 848,750$
$V_{Rd,c} = 592,841.64 N$
$V_{Rd,c} = 592.8 kN$

The shear capacity of the first sample beam – Beam – 2 is 592.8kN.

Beam - 3

For the second sample beam, Beam – 2 the shear capacity is determined as follows as per the simplified formula given by Bazant and his team [20].

$$V_{Rd,c} = [0.2\rho^{3/8}(1+d/a)\sqrt{f_c'}(1+d/d_o)^{-1/2}]b_W d$$

$$d_o = 694\sqrt{d_a}\,(f_c')^{-2/3}$$

Where:

$f_c' = 40MPa$

$d = D - x$; where x is the distance to tensile reinforcement centroid measured from the bottom of the beam cross section.

Assuming there are 3 bars in each layer and there is a clear distance of 30mm between the layers of the reinforcement and also assuming a reinforcement cover of 30mm.

$$x = \frac{3*(30+\frac{30}{2})+3*(30+30+30+\frac{30}{2})+3*(30+30+30+30+30+\frac{30}{2})}{9}$$

$$x = \frac{135+315+495}{9}$$

$$x = 105mm$$

Therefore;

$$d = D - x$$

$$d = 3000mm - 105mm$$

$$d = 2895mm$$

$a = 12,000mm$

$$\rho_l = \frac{A_{sl}}{b_W d} \le 0.02$$

$A_{sl} = 9*\frac{\pi*30^2}{4} = 6361.73mm^2$ is the area of the tensile reinforcement

$$\rho_l = \frac{A_{sl}}{b_W d} \le 0.02$$

$$\rho_l = \frac{6361.73}{250*2895} = 8.79*10^{-3}$$

$b_W = 250mm$

$\sigma_{cp} = 0$

$d_o = 694\sqrt{d_a}\,(f_c')^{-2/3}$

$d_a = 20mm$

$d_o = 694\sqrt{20}\,(40)^{-2/3}$

$d_o = 265.36$

$V_{Rd,c} = [0.2\rho^{3/8}(1+d/a)\sqrt{f_c'}(1+d/d_o)^{-1/2}]b_W d$

$V_{Rd,c} = [0.2(8.79*10^{-3})^{3/8}(1+2895/12000)\sqrt{40}(1+2895/265.36)^{-1/2}]*250*2895$

$V_{Rd,c} = [0.2(0.17)(1+0.241)*\sqrt{40}*(1+10.91)^{-1/2}]*723,750$

$V_{Rd,c} = [0.2(0.17)(1.241)*\sqrt{40}*0.29]*723,750$

$V_{Rd,c} = 560,102.29N$

$V_{Rd,c} = 560.1kN$

The shear capacity of the first sample beam – Beam – 3 is 560.1kN.

Beam - 4

For the second sample beam, Beam – 2 the shear capacity is determined as follows as per the simplified formula given by Bazant and his team [20].

$V_{Rd,c} = [0.2\rho^{3/8}(1+d/a)\sqrt{f_c'}(1+d/d_o)^{-1/2}]b_W d$

$d_o = 694\sqrt{d_a}\,(f_c')^{-2/3}$

Where:

$f_c' = 40MPa$

$d = D - x$; where x is the distance to tensile reinforcement centroid measured from the bottom of the beam cross section.

Assuming there are 3 bars in each layer and there is a clear distance of 30mm between the layers of the reinforcement and also assuming a reinforcement cover of 30mm.

$$x = \frac{3*(30+\frac{30}{2})+3*(30+30+30+\frac{30}{2})+3*(30+30+30+30+30+\frac{30}{2})}{9}$$

$$x = \frac{135+315+495}{9}$$

$$x = 105mm$$

Therefore;

$$d = D - x$$
$$d = 2500mm - 105mm$$
$$d = 2395mm$$

$$a = 12,000mm$$

$$\rho_l = \frac{A_{sl}}{b_W d} \leq 0.02$$

$A_{sl} = 9*\frac{\pi*30^2}{4} = 6361.73mm^2$ is the area of the tensile reinforcement

$$\rho_l = \frac{A_{sl}}{b_W d} \leq 0.02$$
$$\rho_l = \frac{6361.73}{250*2395} = 0.01063$$

$$b_W = 250mm$$

$$\sigma_{cp} = 0$$

$$d_o = 694\sqrt{d_a}\left(f_c'\right)^{-2/3}$$

$$d_a = 20mm$$

$$d_o = 694\sqrt{20}\left(40\right)^{-2/3}$$
$$d_o = 265.36$$

$$V_{Rd,c} = [0.2\rho^{3/8}(1+d/a)\sqrt{f_c'}(1+d/d_o)^{-1/2}]b_W d$$
$$V_{Rd,c} = [0.2(0.01063)^{3/8}(1+2395/12000)\sqrt{40}(1+2395/265.36)^{-1/2}]*250*2395$$
$$V_{Rd,c} = [0.2(0.182)(1+0.2)*\sqrt{40}*(1+9.03)^{-1/2}]*598,750$$
$$V_{Rd,c} = [0.2(0.182)(1.2)*\sqrt{40}*0.32]*598,750$$
$$V_{Rd,c} = 529,307.6N$$
$$V_{Rd,c} = 529.3kN$$

The shear capacity of the fourth sample beam – Beam – 4 is 529.3kN.

Beam - 5

For the fifth sample beam, Beam – 5 the shear capacity is determined as follows as per the simplified formula given by Bazant and his team [20].

$$V_{Rd,c} = [0.2\rho^{3/8}(1+d/a)\sqrt{f_c'}(1+d/d_o)^{-1/2}]b_W d$$
$$d_o = 694\sqrt{d_a}\,(f_c')^{-2/3}$$

Where:

$f_c' = 40MPa$

$d = D - x$; where x is the distance to tensile reinforcement centroid measured from the bottom of the beam cross section.

Assuming there are 3 bars in each layer and there is a clear distance of 30mm between the layers of the reinforcement and also assuming a reinforcement cover of 30mm.

$$x = \frac{3*(30+\frac{30}{2})+3*(30+30+30+\frac{30}{2})+3*(30+30+30+30+30+\frac{30}{2})}{9}$$
$$x = \frac{135+315+495}{9}$$
$$x = 105mm$$

Therefore;

$d = D - x$

$d = 2000mm - 105mm$

$d = 1895mm$

$a = 12,000mm$

$\rho_l = \frac{A_{sl}}{b_W d} \leq 0.02$

$A_{sl} = 9 * \frac{\pi * 30^2}{4} = 6361.73mm^2$ is the area of the tensile reinforcement

$\rho_l = \frac{A_{sl}}{b_W d} \leq 0.02$

$\rho_l = \frac{6361.73}{250 * 1895} = 0.01343$

$b_W = 250mm$

$\sigma_{cp} = 0$

$d_o = 694\sqrt{d_a}\left(f_c'\right)^{-2/3}$

$d_a = 20mm$

$d_o = 694\sqrt{20}\left(40\right)^{-2/3}$

$d_o = 265.36$

$V_{Rd,c} = [0.2\rho^{3/8}(1 + d/a)\sqrt{f_c'}(1 + d/d_o)^{-1/2}]b_W d$

$V_{Rd,c} = [0.2(0.01343)^{3/8}(1 + 1895/12000)\sqrt{40}(1 + 1895/265.36)^{-1/2}] * 250 * 1895$

$V_{Rd,c} = [0.2(0.199)(1 + 0.16) * \sqrt{40} * (1 + 7.14)^{-1/2}] * 473,750$

$V_{Rd,c} = [0.2(0.199)(1.16) * \sqrt{40} * 0.35] * 473,750$

$V_{Rd,c} = 484,159.4N$

$V_{Rd,c} = 484.2kN$

The shear capacity of the fifth sample beam – Beam – 5 is 484.2kN.

ES EN 1992:2015

Beam - 2

For the second sample beam, Beam – 2 the shear capacity is determined as follows as per the Ethiopian Standard – Based on Euro Norms.

$$V_{Rd,c} = [C_{Rd,c} k (100 \rho_l f_{ck})^{1/3} + k_1 \sigma_{cp}] b_W d$$

Where:

$$f_{ck} = 40 MPa$$

$$k = 1 + \sqrt{\frac{200}{d}} \leq 2.0 \text{ with}$$

$d = D - x$; where x is the distance to tensile reinforcement centroid measured from the bottom of the beam cross section.

With similar assumption as mentioned in the analysis procedure for Beam - 1

$$x = 105 mm$$

Therefore;

$$d = D - x$$
$$d = 3500 mm - 105 mm$$
$$d = 3395 mm$$

$$k = 1 + \sqrt{\frac{200}{3395}} \leq 2.0$$
$$k = 1.243$$

$$\rho_l = \frac{A_{sl}}{b_W d} \leq 0.02$$

$A_{sl} = 9 * \frac{\pi * 30^2}{4} = 6361.73 mm^2$ is the area of the tensile reinforcement

$$\rho_l = \frac{A_{sl}}{b_W d} \le 0.02$$

$$\rho_l = \frac{6361.73}{250*3395} = 7.495*10^{-3}$$

$$b_W = 250mm$$

$$\sigma_{cp} = 0$$

$$C_{Rd,c} = \frac{0.18}{\gamma_c} = \frac{0.18}{1.5} = 0.12$$

$$k_1 = 0.15$$

$$v_{\min} = 0.035k^{3/2} f_{ck}^{1/2}$$
$$v_{\min} = 0.035(1.243)^{3/2}(40)^{1/2}$$
$$v_{\min} = 0.307$$
$$V_{\min} = 0.307*250*3395$$
$$V_{\min} = 260566.25N$$
$$V_{\min} = 260.57kN$$

$$V_{Rd,c} = [C_{Rd,c}k(100\rho_l f_{ck})^{1/3} + k_1\sigma_{cp}]b_W d$$
$$V_{Rd,c} = [0.12*1.243(100*7.495*10^{-3}*40)^{1/3} + 0]250*3395$$
$$V_{Rd,c} = 0.463*848750$$
$$V_{Rd,c} = 392971N$$
$$V_{Rd,c} = 392.97kN$$

The shear capacity of the second sample beam – Beam – 2 is 392.97kN.

Beam - 3

For the third sample beam, Beam – 3 the shear capacity is determined as follows as per the Ethiopian Standard – Based on Euro Norms.

$$V_{Rd,c} = [C_{Rd,c}k(100\rho_l f_{ck})^{1/3} + k_1\sigma_{cp}]b_W d$$

Where:

$f_{ck} = 40MPa$

$k = 1 + \sqrt{\frac{200}{d}} \leq 2.0$ with

$d = D - x$; where x is the distance to tensile reinforcement centroid measured from the bottom of the beam cross section.

With similar assumption as mentioned in the analysis procedure for Beam - 1

$x = 105mm$

Therefore;

$d = D - x$
$d = 3000mm - 105mm$
$d = 2895mm$

$k = 1 + \sqrt{\frac{200}{2895}} \leq 2.0$
$k = 1.263$

$\rho_l = \frac{A_{sl}}{b_W d} \leq 0.02$

$A_{sl} = 9 * \frac{\pi * 30^2}{4} = 6361.73mm^2$ is the area of the tensile reinforcement

$\rho_l = \frac{A_{sl}}{b_W d} \leq 0.02$
$\rho_l = \frac{6361.73}{250 * 2895} = 8.79 * 10^{-3}$

$b_W = 250mm$

$\sigma_{cp} = 0$

$C_{Rd,c} = \frac{0.18}{\gamma_c} = \frac{0.18}{1.5} = 0.12$

$k_1 = 0.15$

$v_{\min} = 0.035k^{3/2} f_{ck}^{1/2}$

$v_{\min} = 0.035(1.263)^{3/2}(40)^{1/2}$

$v_{\min} = 0.314$

$V_{\min} = 0.314 * 250 * 2895$

$V_{\min} = 227257.5N$

$V_{\min} = 227.26kN$

$V_{Rd,c} = [C_{Rd,c} k(100\rho_l f_{ck})^{1/3} + k_1 \sigma_{cp}] b_W d$

$V_{Rd,c} = [0.12 * 1.263(100 * 8.79 * 10^{-3} * 40)^{1/3} + 0]250 * 2895$

$V_{Rd,c} = 0.497 * 723750$

$V_{Rd,c} = 359703N$

$V_{Rd,c} = 359.7kN$

The shear capacity of the second sample beam – Beam – 3 is 359.7kN

Beam - 4

For the fourth sample beam, Beam – 4 the shear capacity is determined as follows as per the Ethiopian Standard – Based on Euro Norms.

$V_{Rd,c} = [C_{Rd,c} k(100\rho_l f_{ck})^{1/3} + k_1 \sigma_{cp}] b_W d$

Where:

$f_{ck} = 40MPa$

$k = 1 + \sqrt{\frac{200}{d}} \leq 2.0$ with

$d = D - x$; where x is the distance to tensile reinforcement centroid measured from the bottom of the beam cross section.

With similar assumption as mentioned in the analysis procedure for Beam - 1

$x = 105mm$

Therefore;

$$d = D - x$$
$$d = 2500mm - 105mm$$
$$d = 2395mm$$

$$k = 1 + \sqrt{\frac{200}{2395}} \leq 2.0$$
$$k = 1.289$$

$$\rho_l = \frac{A_{sl}}{b_W d} \leq 0.02$$

$A_{sl} = 9 * \frac{\pi * 30^2}{4} = 6361.73mm^2$ is the area of the tensile reinforcement

$$\rho_l = \frac{A_{sl}}{b_W d} \leq 0.02$$
$$\rho_l = \frac{6361.73}{250 * 2395} = 1.06 * 10^{-2}$$

$$b_W = 250mm$$

$$\sigma_{cp} = 0$$

$$C_{Rd,c} = \frac{0.18}{\gamma_c} = \frac{0.18}{1.5} = 0.12$$

$$k_1 = 0.15$$

$$v_{\min} = 0.035 k^{3/2} f_{ck}^{1/2}$$
$$v_{\min} = 0.035 (1.289)^{3/2} (40)^{1/2}$$
$$v_{\min} = 0.324$$

Beam – 2

$$V_c = 2\sqrt{f_c'}b_w d$$
$$V_c = \frac{2\sqrt{5801.51psi} * 9.843" * 133.661"}{1000 lb/kip}$$
$$V_c = 200.416kip$$
$$V_c = 891.49kN$$

The shear capacity of the second sample beam – Beam – 2 is 891.49kN.

Beam – 3

$$V_c = 2\sqrt{f_c'}b_w d$$
$$V_c = \frac{2\sqrt{5801.51psi} * 9.843" * 113.976"}{1000 lb/kip}$$
$$V_c = 170.9kip$$
$$V_c = 760.2kN$$

The shear capacity of the third sample beam – Beam – 3 is 760.2kN.

Beam – 4

$$V_c = 2\sqrt{f_c'}b_w d$$
$$V_c = \frac{2\sqrt{5801.51psi} * 9.843" * 94.291"}{1000 lb/kip}$$
$$V_c = 141.383kip$$
$$V_c = 628.9kN$$

The shear capacity of the fourth sample beam – Beam – 4 is 628.9kN.

$$V_{Rd,c} = [C_{Rd,c} k (100\rho_l f_{ck})^{1/3} + k_1 \sigma_{cp}] b_W d$$
$$V_{Rd,c} = [0.12 * 1.289 (100 * 1.06 * 10^{-2} * 40)^{1/3} + 0] 250 * 2395$$
$$V_{Rd,c} = 0.539 * 598750$$
$$V_{Rd,c} = 322726N$$
$$V_{Rd,c} = 322.73kN$$

The shear capacity of the second sample beam – Beam – 4 is 322.73kN

APPENDIX B

Results of Numerical Program based on ES EN 1992:2015 and ACI 318

Table A-1: Beam - 2 Shear Capacity - ES EN

Beam shear capacity

BEAM - 2

Beam cross section	
B (mm)	250
H (mm)	3500
x	105
Cover (mm)	30
d (mm)	3395
Beam Concrete Grade	
f_{cu} (Mpa)	50
f_{ck} (Mpa)	40
f_{cd} (Mpa)	22.67

$C_{Rd,c}$	0.12
k	1.2428
k_1	0.15
Beam Tensile Reinforcement	9 ϕ 30
A_s (mm^2)	6361.73
ρ	0.007495
σ_{cp} (Mpa)	0
v_{min} (Mpa)	0.3067
$V_{Rd,c}$ (N)	393230.7
$V_{Rd,c}$ (kN)	393.231

Table A-2: Beam - 3 Shear Capacity - ES EN

Beam shear capacity

BEAM - 3

Beam cross section	
B (mm)	250
H (mm)	3000
x	105
Cover (mm)	30
d (mm)	2895
Beam Concrete Grade	
f_{cu} (Mpa)	50
f_{ck} (Mpa)	40
f_{cd} (Mpa)	22.67

$C_{Rd,c}$	0.12
k	1.2629
k_1	0.15
Beam Tensile Reinforcement	9 ϕ 30
A_s (mm^2)	6361.73
ρ	0.00879
σ_{cp} (Mpa)	0
v_{min} (Mpa)	0.3142
$V_{Rd,c}$ (N)	359325.2
$V_{Rd,c}$ (kN)	359.326

Table A-3: Beam - 4 Shear Capacity - ES EN

Beam shear capacity			
BEAM - 4			
Beam cross section		$C_{Rd,c}$	0.12
B (mm)	250	k	1.289
H (mm)	2500	k_1	0.15
x	105	Beam Tensile Reinforcement	9 ϕ 30
Cover (mm)	30	A_s (mm^2)	6361.73
d (mm)	2395	ρ	0.010625
Beam Concrete Grade		σ_{cp} (Mpa)	0
f_{cu} (Mpa)	50	v_{min} (Mpa)	0.324
f_{ck} (Mpa)	40	$V_{Rd,c}$ (N)	323203.7
f_{cd} (Mpa)	22.67	$V_{Rd,c}$ (kN)	323.204

Table A-4: Beam - 5 Shear Capacity - ES EN

Beam shear capacity			
BEAM - 5			
Beam cross section		$C_{Rd,c}$	0.12
B (mm)	250	k	1.3249
H (mm)	2000	k_1	0.15
x	105	Beam Tensile Reinforcement	9 ϕ 30
Cover (mm)	30	A_s (mm^2)	6361.73
d (mm)	1895	ρ	0.013428
Beam Concrete Grade		σ_{cp} (Mpa)	0
f_{cu} (Mpa)	50	v_{min} (Mpa)	0.3376
f_{ck} (Mpa)	40	$V_{Rd,c}$ (N)	284190.1
f_{cd} (Mpa)	22.67	$V_{Rd,c}$ (kN)	284.191

Table A-5: Beam - 2 Shear Capacity - ACI

Beam shear capacity	
BEAM - 2	
Beam cross section	
B (in)	9.843
H (in)	137.796
x (in)	4.134
Cover (in)	1.181102
d (in)	133.6614
Beam Concrete Grade	
f_{ck} (psi)	5801.52
$V_{Rd,c}$ (kip)	200.4169
$V_{Rd,c}$ (kN)	891.495

Table A-6: Beam - 3 Shear Capacity - ACI

Beam shear capacity	
BEAM - 3	
Beam cross section	
B (in)	9.843
H (in)	118.111
x (in)	4.134
Cover (in)	1.181102
d (in)	113.9764
Beam Concrete Grade	
f_{ck} (psi)	5801.52
$V_{Rd,c}$ (kip)	170.9005
$V_{Rd,c}$ (kN)	760.2

Table A-7: Beam - 4 Shear Capacity - ACI

Beam shear capacity	
BEAM - 4	
Beam cross section	
B (in)	9.843
H (in)	98.426
x (in)	4.134
Cover (in)	1.181102
d (in)	94.29134
Beam Concrete Grade	
f_{ck} (psi)	5801.52
$V_{Rd,c}$ (kip)	141.384
$V_{Rd,c}$ (kN)	628.905

Table A-8: Beam - 5 Shear Capacity - ACI

Beam shear capacity	
BEAM - 5	
Beam cross section	
B (in)	9.843
H (in)	78.741
x (in)	4.134
Cover (in)	1.181102
d (in)	74.6063
Beam Concrete Grade	
f_{ck} (psi)	5801.52
$V_{Rd,c}$ (kip)	111.8675
$V_{Rd,c}$ (kN)	497.609

APPENDIX C

Fortran Program prepared based on ES EN 1992:2015 and ACI 318

Below is shown few analysis outputs of a Fortran V.97 program intended for the prediction of shear capacity of the sample reinforced concrete beams using both the ES EN and ACI building codes.

```
! The shear capacity of a reinforced concrete beam is calculated
! The calculation is based on both ES EN and ACI

double precision:: bw, h
double precision:: n,fi,l,As,x,k
double precision:: fck
double precision :: lamda

lamda=1d0

print*,"Write beam width(mm), beam depth(mm) "
read*, bw,h
print*,"write number of reinforcement bars,bar diameter(mm),bar
layers"
read*,n,fi,l
print*,"write the cylindrical compressive strength of the
concrete(MPa)"
read*,fck
As=(acos(-1d0)*fi**2/4)*n
x=105
deff=h-x
rho=As/(bw*deff)
k=1+sqrt(200/deff)


Vrd_ES=(0.12d0*k*((100d0*rho*fck)**(1d0/3d0)))*bw*deff
Vrd_ACI=(2*lamda*sqrt(fck*145.038)*(bw/25.4)*(deff/25.4))/1000

print*,"The shear capacity as per ES EN is =",Vrd_ES/1000,"kN"
print*,"The shear capacity as per ACI is =",Vrd_ACI*4.4482,"kN"

end
```

Having compiled the Fortran program presented above which is intended for the calculation of shear capacity of the sample reinforced concrete beams, the following results were obtained:

```
nahom@nahom-Satellite-C55-C:~$ cd MSc_Comp_21/
nahom@nahom-Satellite-C55-C:~/MSc_Comp_21$ gfortran -ffree-form
Eng_Shear_Capacity.f90
nahom@nahom-Satellite-C55-C:~/MSc_Comp_21$ ./a.out
 Write beam width(mm), beam depth(mm)
```

```
250,4000
 write number of reinforcement bars,bar diameter(mm),bar layers
9,30,3
 write the cylindrical compressive strength of the concrete(MPa)
40
 The shear capacity as per ES EN is =   425.331665     kN
 The shear capacity as per ACI is =   1022.74011     kN
nahom@nahom-Satellite-C55-C:~/MSc_Comp_21$ gfortran -ffree-form
Eng_Shear_Capacity.f90
nahom@nahom-Satellite-C55-C:~/MSc_Comp_21$ ./a.out
 Write beam width(mm), beam depth(mm)
250,3500
 write number of reinforcement bars,bar diameter(mm),bar layers
9,30,3
 write the cylindrical compressive strength of the concrete(MPa)
40
 The shear capacity as per ES EN is =   393.203430     kN
 The shear capacity as per ACI is =   891.451294     kN
nahom@nahom-Satellite-C55-C:~/MSc_Comp_21$ gfortran -ffree-form
Eng_Shear_Capacity.f90
nahom@nahom-Satellite-C55-C:~/MSc_Comp_21$ ./a.out
 Write beam width(mm), beam depth(mm)
250,3000
 write number of reinforcement bars,bar diameter(mm),bar layers
9,30,3
 write the cylindrical compressive strength of the concrete(MPa)
40
 The shear capacity as per ES EN is =   359.307892     kN
 The shear capacity as per ACI is =   760.162354     kN
nahom@nahom-Satellite-C55-C:~/MSc_Comp_21$ gfortran -ffree-form
Eng_Shear_Capacity.f90
nahom@nahom-Satellite-C55-C:~/MSc_Comp_21$ ./a.out
 Write beam width(mm), beam depth(mm)
250,2500
 write number of reinforcement bars,bar diameter(mm),bar layers
9,30,3
 write the cylindrical compressive strength of the concrete(MPa)
40
 The shear capacity as per ES EN is =   323.197632     kN
 The shear capacity as per ACI is =   628.873535     kN
nahom@nahom-Satellite-C55-C:~/MSc_Comp_21$ gfortran -ffree-form
Eng_Shear_Capacity.f90
nahom@nahom-Satellite-C55-C:~/MSc_Comp_21$ ./a.out
 Write beam width(mm), beam depth(mm)
250,2000
 write number of reinforcement bars,bar diameter(mm),bar layers
9,30,3
 write the cylindrical compressive strength of the concrete(MPa)
40
 The shear capacity as per ES EN is =   284.183685     kN
 The shear capacity as per ACI is =   497.584717     kN
```

It can be readily seen that the shear capacity determination using the analytic calculation presented at the beginning of the two sub topics under this chapter and those using

numerical programs using both excel and Fortran V.97 give sufficiently compatible results for the corresponding sample beams and design codes.